SATELLITE MICROWAVE OBSERVATIONS OF A STORM COMPLEX: A COMPARATIVE ANALYSIS

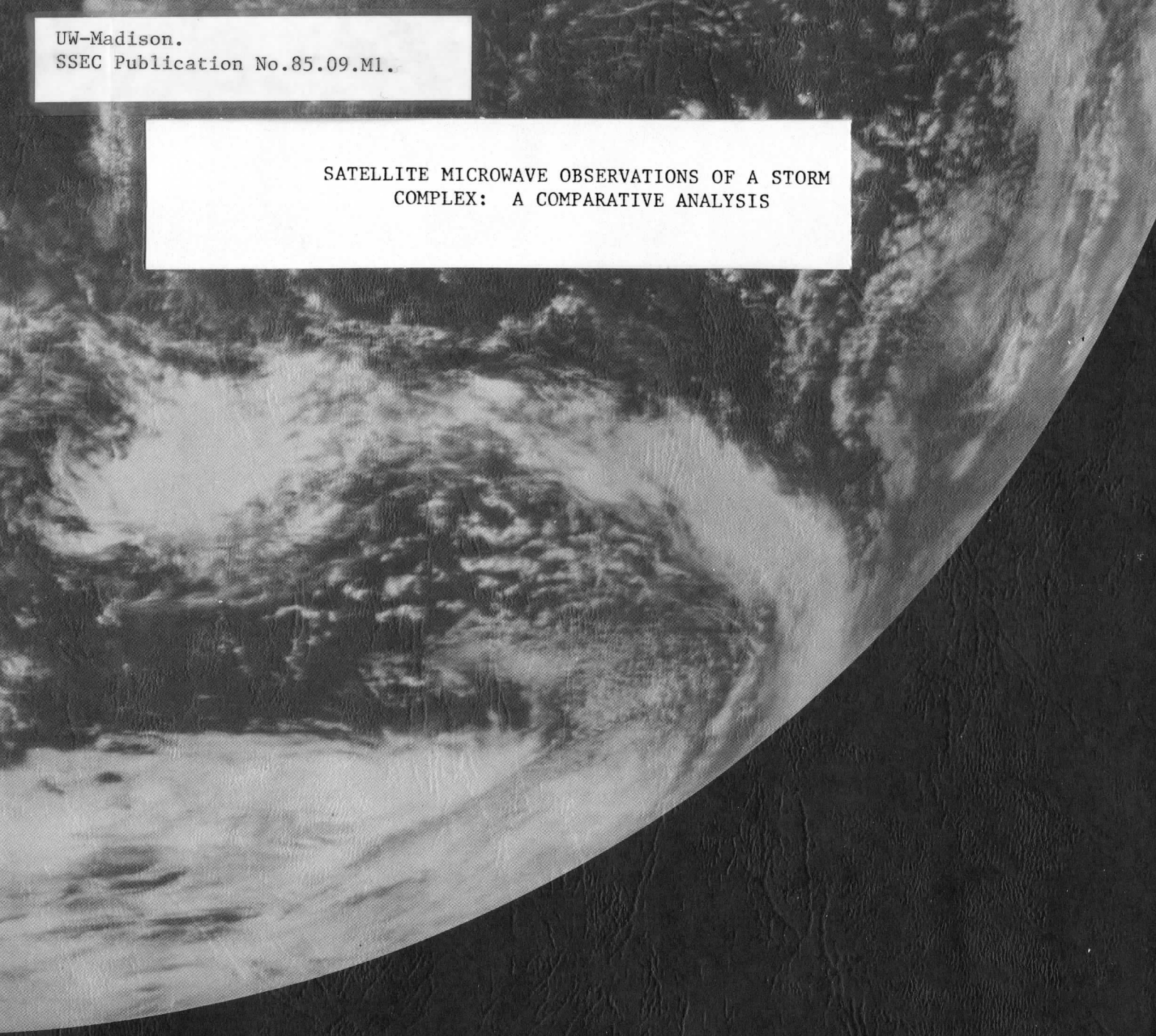

A REPORT

from the space science and engineering center
the university of wisconsin-madison
madison, wisconsin

SATELLITE MICROWAVE OBSERVATIONS OF A STORM COMPLEX: A COMPARATIVE ANALYSIS

An Interim Report to

National Aeronautics and Space Administration

Grant #NAG 5-391

University Account #144U071

for the period of

1 February 1984 to 30 April 1985

Submitted by

David W. Martin

Space Science and Engineering Center
at the University of Wisconsin-Madison
1225 West Dayton Street
Madison, Wisconsin 53706
(608) 262-0544

September 1985

Satellite Microwave Observations of a Storm Complex: A Comparative Analysis

1. Introduction

The 1983 paper of Spencer et al. drew attention to an anomalous observation of the Nimbus 7 Scanning Multichannel Microwave Radiometer (SMMR). Looking at rain over Kansas at 37 GHz, SMMR recorded a brightness temperature 60 to 65°C colder than the coldest values predicted by the conventional theory of rain over land. In this case, and in others presented in the paper, the "cold event" was found to be co-located with a tall, highly reflective radar echo. It was found, further, that in a qualitative sense the cold events could be explained as a depletion, through scattering by ice particles, of upwelling microwave radiation emitted by a lower rain layer. Spencer and his colleagues concluded that the association of cold events with rain offered hope of inferring heavy rates over land from passive microwave instruments like SMMR. They also raised the possibility that the more extreme of the cold events might so consistently be associated with very intense convection that SMMR could be useful in detecting severe storms.

The present work extends the previous analysis. It tests the hypothesis that cold events of the kind just described correspond to a particular stage in a class of thunderstorms. That class is storms whose updrafts are (a) strong, broad and moist and (b) extend well above the freezing level. Condition (a) implies strong mesoscale forcing. Condition (b) implies a tall updraft or a relatively low freezing level. Such storms should have big, intense radar echoes and cold, fast-growing anvils.

The selection of a case for study was governed by the coincidence of a SMMR cold event with radar and GOES image sequences. Once a case had been selected and the event had been described, the analysis proceeded through radar, raingauge and GOES infrared observations. Because it has become a standard tool for the detection of thunderstorms, radar was the starting point for the definition of the hypothesized storm. The radar signature then was compared to the signature of the storm in raingauge observations, satellite infrared images and, finally, satellite microwave images.

2. Satellite microwave observations

SMMR data from one year--1979--were available. As part of a statistical study of the association of cold events with severe weather (Spencer et al., 1985), these data were scanned (by computer) for low 37 GHz temperatures, small 37 GHz polarization temperature differences, and warm 18 GHz temperatures relative to those at 37 GHz. From printouts of brightness temperature (T_B) for the events so identified, several extreme cold events were noted. From these, using the criteria stated above, one case was chosen for intensive study. This case occurred early on 23 June 1979, close to the western edge of the Ozark Plateau. It was distinguished from the other cold events in having an exceptionally low minimum temperature at 37 GHz (181 K in the horizontal polarization). Of further interest was its association in a radar summary chart with a large echo system. The coldest footprint appeared to be matched to a strong echo cell. However, no event of corresponding coldness could be found to match a second strong cell which was close to the first.

SMMR scanned the echo cluster at 0047 CST (in this paper all times are Central Standard). Images in two polarizations (horizontal and vertical)

in each of five frequencies (6.6, 10.6, 18, 21 and 37 GHz) were available in TCT format.[1] These images are shown in Fig. 1, which includes state boundaries, the location of the Monett, Missouri National Weather Service WSR-57 radar and 40 and 220 km range circles from that radar. SMMR data have been remapped to the projection appropriate to a geostationary satellite at the position of GOES-East on 23 June 1979 (0°N, 75°W). By means of overlay comparisons of the 37 GHz images with Lake Michigan and Gulf of Mexico coastlines we were able to improve the absolute location accuracy of all channels of the SMMR data to a fraction of a 37 GHz footprint.

The 181 K cold event (hereafter referred to as E1) was located along the Kansas-Missouri border. At 37 GHz (Fig. 1a,b; also see Fig. 2a,b) it was centered in Missouri just inside the Kansas border and was elongated east and west. Neighboring cold events, both just within the 200 km radar range line, lay 30 km to the northwest (E2) and 220 km to the southwest (E3). The lowest H-polarization temperatures with these features (220 K and 214 K, for E2 and E3, respectively) were at least 30°C warmer than that of E1. Although more than a dozen reservoirs are located within range of the Monett radar (e.g., see Espenshade and Morrison, 1974), none are close to the cold events.

The events "slump" with each step toward a lower frequency. Between 37 and 21 GHz (Fig. 1, a-d) E1 and E2 melt into a single feature. E3 disappears between 18 and 10.6 GHz (Fig. 1, e-h); E1/E2 virtually disappears between 10.6 and 6.6 GHz (Fig. 1, g-j). Slumping is in part an

---

[1] For more information on SMMR see the contribution of Per Gloerson and Lew Hardis in The Nimbus 7 Users' Guide, Goddard Space Flight Center, Greenbelt, MD, 213-245, 1978.

effect of instrument resolution (note the increasing coarseness of the imagery from 37 through 6.6 GHz). Probably a more important factor, however, is the increasing transparency of rainclouds to microwave radiation as frequency is decreased (e.g., see Fraser, 1979; Savage, 1976; Wu and Weinman, 1984).

With each step toward a lower frequency, E1 (and the merged feature, E1/E2) shifts toward the west. This "frequency migration" of a cold event may be due to the frequency dependence of transparency (as described above) working in parallel with a second factor. Grody (1984) has noted that for wet soils emissivity decreases as frequency decreases. Therefore a gradient in soil moisture, wetter toward the west, could, in conjunction with higher rain transparency at lower frequencies, produce an effect like that which was observed.

Spencer et al. (1983) found that their storms were slightly, but consistently, more polarized than the rain-free areas around. Images of polarization temperature difference (δT_b; V-H) are shown in Fig. 3 for four frequencies. For one frequency, 37 GHz, δT_b also has been mapped (Fig. 4). Each image is dominated by structure at or smaller than the scale of the footprint corresponding to the respective frequency. At 37 GHz this structure is due to a one-quarter footprint offset between the V and H channels. At the remaining frequencies this structure is due mainly to an alternation between polarizations from one scan to the next (Njoku et al., 1980).

Otherwise at 37 GHz there are two main centers of large δT_b, one straddling the Missouri-Kansas border and the other in Oklahoma. The Missouri-Kansas center itself has, albeit weakly, two parts, which straddle the 38th parallel.

The main centers of large δT_b (including the two parts of the Missouri-Kansas center) coincide with the three cold events E1, E2 and E3.

Apart from footprint-sized cells (where δT_b reaches 25°C) the largest values of δT_b are about 15°C. This is somewhat larger than the value (11°C) reported by Spencer at al. (1983) for the Kansas storm; however, even the local peak values are much smaller than the 50 to 60°C values which are typical for lakes and seas.

Centers of δT_b emerge from a comparatively flat background. Excepting minor centers of somewhat larger δT_b (for example, the center which straddles the Missouri-Arkansas border southeast of Monett), which appear to be associated with larger reservoirs, background values lie mostly between 5° and 10°C.

As might be expected, with each step towards lower frequency (Fig. 3, a-d) the main centers slump. At 10.6 GHz (Fig. 3c) both have virtually disappeared. In their place is a gradient of δT_b, with higher values toward the west. Such a gradient is consistent with the suggestion made above that soils may have been wetter in that direction.

3. Radar echoes

The National Weather Service radar summary chart mentioned above was valid for 0035, twelve minutes before the SMMR overpass. The part of that chart which is presented in Fig. 5 shows a comma-shaped echo--the "large" system mentioned above--centered in Kansas and Oklahoma. An isolated cell of level-5 intensity was located within the comma in north-central Oklahoma and a level-5 cell couplet straddled the Kansas-Missouri border. Echo tops with the Oklahoma cell and the Kansas part of the couplet peaked at 16.2 km (53,000 feet). The peak top reported for the Missouri part of the couplet,

13.4 km (44,000 feet), was distinctly lower; this cell also had the smallest level-5 core.

The comma echo was moving east at 15 m s^{-1}. Intensities in the stronger cells were either steady or increasing.

Three reports of severe weather were recorded for this system in Storm Data (NOAA, 1979): at 0000 a windstorm, at 0015 a funnel cloud and at 0130 a flash flood. Each of these storm events occurred within or close to the Oklahoma cell. A mail survey of weekly newspapers uncovered one other report. As columnist for a newspaper in Liberal, Missouri (37°36'N, 94°30'W; see Fig. 5), Mr. Willis W. Strong (personal communication) reported on "heavy rain, wind and lightning" which "moved in late Friday [22 June] and lasted for about 3 hours....This area received about 2 inches--some places nearby had 6 to 8 inches of rain."

On Fig. 5 we also show the locations of the coldest footprints within each of the three SMMR cold events. All three coldest footprints fall within the comma echo; in fact, all fall on or within the VIP level-3 contour. Although none falls within any of the three level-5 contours which are present in the tail of the comma echo, for the two most extreme (i.e., coldest) footprints (E1 and E3) there is a close association with tall, intense cells: E1 with the Kansas-Missouri cell couplet and E3 with the Oklahoma cell.

In Fig. 5, Liberal, Missouri lies along the axis of the Kansas-Missouri couplet and within the E1 coldest footprint. Certainly eastward movement of the comma echo is consistent with the westward increase in soil moisture which was postulated above to explain the westward lapse in T at lower frequencies.

Apart from the radar summary chart, only the Monett, Missouri radar provided useful observations of the three cold events. For the Monett radar (36°53'N, 93°54'W) quality photographs of the plan position indicator (ppi) scope were available on 16 mm microfilm beginning at 0019. Prints were made of a subset of these microfilm images covering, at 4 min time resolution, the period between 0019 and 0111. Within this period lies a SMMR-radar "overlap interval". This overlap interval represents the period during which the column of raindrops and ice particles which might be present in any given SMMR footprint could be expected to fall through a radar beam the center of which is up to 5 km above the ground (e.g., see Spencer and Grody, 1985). For echo tops near 15 km and raindrop and ice particle fallspeeds near 15 m s^{-1}, the overlap interval as it is here defined would cover the ¼ h from 0047 through 0100. If SMMR is truly "seeing" raindrops and ice particles, it is over this interval that we would expect to find the closest link between satellite brightness temperatures and radar reflectivities.

To isolate the larger scales of reflectivity structure we look at echo groups. Here "echo group" is defined as a clump of echoes which in terms of distance and intensity is distinct from other echoes or clumps of echoes and in terms of time is coherent. If echo group boundaries are drawn so that every significant echo in each print of the series is included in one and only one group, we come to the classification which is shown in Fig. 6. Five echo groups (M1, K1, K2, 01 and 02) were identified. One of these echo groups (02) appeared during the period of the series. It proved to be of little significance and hereafter for the most part is treated as part of K2. Group 01 corresponds to the Oklahoma cell in Fig. 5, K2 to the western part of the Kansas-Missouri couplet, M1 to the eastern part of that

couplet and K1 to a part of the comma echo extending north from the couplet. VIP level-1 echo connected all of the groups throughout the period; however, in spite of the 0035 radar summary chart (Fig. 5) no group was ever connected to another by echo higher than VIP level 2. Peak VIP levels for one echo group (01), which remained largely between the 185 and 232 km range lines, may have been underestimated by the Monett radar.

At 0047 and across the overlap period one echo group--M1--stood out. Consistently it had the highest echo intensity (VIP level-5). Consistently, too, M1 had the largest area at an intermediate intensity, level-3. In terms of a peak intensity and sustaining a high peak intensity, K1 was most like M1. K2 was noteable for shrinking area at level-3 intensity.

4. Rainfall

As a first guess of the SMMR-coincident rain field, gauge measurements of rain falling in the hour ending at 0100 were analyzed over and around the SMMR cold events (Fig. 7). Hourly rainfall yielded a bi-cellular pattern, with one rain center in Oklahoma and the other, larger rain center mainly in Kansas. The Kansas center was lobed. One lobe extended east into Missouri, another northwest and a third southwest toward the Oklahoma center. Rain rates peaked at 51 mm h^{-1}; they were highest in the Oklahoma center.

The Oklahoma center corresponds to echo group 01; the east and northwest lobes of the Kansas rain center correspond respectively to echo groups M1 and K1; and the core and southwest lobe of the Kansas center correspond to group K2. But for both centers the network is thinnest where the rain is heaviest, and from the gauge observations alone little can be

said about the SMMR-scale structure of this storm.

By hand, a subset of the microfilm radar reflectivity images was converted to rain rate images. Except that (1) the resolution of the resulting digital radar rain images was 10 km rather than 20 km and (2) no data were taken within 50 km of the radar, the procedure followed was that described by Spencer (1984). Eleven were digitized, beginning with the image for 0019 and continuing at roughly 4 min intervals through 0059. Before being analyzed, these digital images were remapped to a GOES projection.

The average of the eleven images, shown in Fig. 8, agrees with the gauge map in indicating two main rain centers, with a weak bridge between; however, in intensity it emphasizes the Kansas rain center over the Oklahoma center. Fig. 8 also emphasizes the structure in the Kansas rain center, which in radar rainfall is not so much a core with three lobes as it is an east-west line of cells and (to the north of the line) an outlier.

Such differences are further magnified in the digital radar rain image for 0047 (Fig. 9). At the time of the Nimbus overpass the easternmost part of the radar-visible rain storm (corresponding to the east lobe of Fig. 7) and the outlier (which has no counterpart in Fig. 7) contained the heaviest rain. Averaged over a $(10\ km)^2$ area the peak rates there were 76 mm h^{-1}.

How good are the radar estimates of rainfall? Spencer (1984) argued that, compared to actual rain rates, for the radars he selected (Monett was one of these) the standard error of estimate--averaged over $(20\ km)^2$ areas--would be not more than 60% of the mean of the actual rain rates. Because a single daily gauge measurement typically represents rainfall over an area smaller than $(20\ km)^2$ (e.g., see Landsberg, 1984), in the present instance we should not expect such a (relatively) high level of agreement.

Moreover, rain from 0019 through 0059 could not be wholly representative of rain through the hour ending at 0100. Still, if we keep these limits in mind, it is possible to evaluate the radar estimates by means of the gauge measurements which have been described above.

In the present case for all gauges within the annulus defined by the 50 km and 215 km radii, radar rainrate was read at the sites of the gauges. For these gauges, a total of 57, the mean rainrate was 2.2 mm h^{-1}. A histogram of differences (Fig. 10) shows a spike on zero and rather long tails. A scatterplot (Fig. 11) indicates a pattern typical for comparisons of point and areal measurements of a hummocky field: radar (areal) overestimate at low rain rates and underestimate at high rain rates. The bias in the present case is 1.2 (radar exceeding gauge).

If we let gauge rainfall be G and radar rainfall be A, the least-squares regression relation, in units of mm, is given by

$$A = \tfrac{1}{2} + 4/5\ G.$$

The correlation coefficient for this relation is an agreeable 0.83. However, the standard error of the estimate, 5.1 mm, is 2.3 rather than 0.6 times larger than the mean gauge rain. Even allowing for differences in the periods of the observations and in the spatial averaging, this result suggests that Spencer's (1984) estimate of the accuracy of manually digitized radar rain rate was optimistic.

5. Cloud-top temperature

A different view of the cold events was afforded by the window-infrared channel on GOES-East. Images were available every half hour, at a nominal resolution of 4 km. Scans of the cold events lagged

each of the nominal image times by about 4 min. The five images centered on 0100 were examined.

Comparing graphics and image coastlines along the Great Lakes and the Gulf of Mexico at 0000 and 0030, we concluded that the GOES navigation at these times was accurate within ±4 km, and at least as accurate as ±8 km throughout the sequence. To correct for satellite parallax--the position offset resulting from a slant view of an elevated object--it was assumed that cloud tops lay near 13 km (for temperatures observed nearby, this corresponds to a pressure level of 175 mb). Then each infrared image was (digitally) shifted 9 km southward and 5 km eastward. As with SMMR, all infrared images shown here are centered on Monett.

Thirteen minutes before the SMMR overpass, a single big, cold canopy of cloud is seen in the infrared channel of GOES-East (Fig. 12). The cold center of this canopy cloud (hereafter, simply referred to as "canopy") was offset to the west of its geometric center. Otherwise the canopy in this view is remarkable for the absence of cumulonimbus-scale structure.

In fact some such structure was present. It emerged when an MB enhancement (Corbell et al., 1979) was applied to the image (Fig. 13). Apparently, this structure was confined to the coldest part of the canopy. Furthermore, it appeared to be present over a range of scales--at the small end apparently including individual pixels. Within the structure region there were 14 more or less distinct minima in temperature. The coldest temperature, which lay north-northwest of Monett, was -69°C (204 K). The range was small, only 8°C. Temperatures along the inside edge of the canopy were about -42°C (230 K).

The infrared MB sequence is shown in Fig. 14. For the canopy as a whole between 0000 and 0200 there is good time continuity. Like the comma echo the canopy was moving. Remarkably enough, its measured velocity was the same: 15 m s^{-1}, toward the east. At moderately cold temperatures--241 K to 231 K--the canopy expanded. By 0130, at colder temperatures, the canopy was shrinking. Structure within the cold area changed rapidly, especially on cumulonimbus and smaller scales.

Beyond any reasonable doubt, the canopy is simply melded cirrus cloud from a small number of cumulonimbi. These cumulonimbi lie mainly to the west of the central axis of the canopy. They are clustered, a condition which creates cold domes within the canopy. They also are impulsive. Occasionally a cumulonimbus top punches through the canopy. Although we do not know whether the canopy endured for a full 6 h, it otherwise qualifies as a mesoscale convective complex (Maddox, 1980).

All of the cold events occurred within the canopy. All occurred within an echo. Whether each of the cold events was associated with an echo group and, if so, whether the echo group associated with the extreme cold event (E1) was in any significant sense unique are questions still to be answered.

6. Cold events

Echo group outlines at 0047 were laid over the H37 GHz SMMR image (Fig. 15). Each of the cold events fell within an echo group outline (E1 with M1, E2 with K2, and E3 with 01). Of the remaining two outlines, K2 is associated with a western spur of cold event E1, and 02 (at this time a small, weak echo system--see Fig. 9) is associated with a minor cold center.

But in Fig. 15 there also is a discrepancy. Echo cores are systematically offset ½ to 1 SMMR footprint to the north of the centers of cold events. No such offset remained after SMMR images had been adjusted in location by means of coastlines. The offset may be explained, however, as an effect of parallax if at 37 GHz scattering by ice elevated the source of the direct beam microwave radiation which SMMR received along its slant path view. In the present case the offset for a scattering layer located at 7 km elevation is 8 km, toward the south. Indeed, when this correction was applied to the H37 image, the discrepancy in locations of echo cores and cold events very nearly disappeared.[2]

Several differences between echo groups are apparent in Fig. 15. For the 1/3 h roughly centered on the SMMR overpass, the more important of these differences have been summarized in Table 1. Of particular interest is M1, which here includes echo group K2. At the time of the SMMR overpass, M1 and K1 shared the distinction of having the peak (digital) rainrate. However, as was implied earlier, the rain area of M1 was unique in size: at rates of 30 to 50 mm h^{-1}, it was several times larger than that of either K1 or O1. At rain rates higher than ~30 mm h^{-1} only M1 had an area significantly larger than 500 km^2, the one-half power area of a SMMR 37 GHz footprint.

Curiously, as cold events E3 was more extreme than E2. Nevertheless, in terms of rainrate K1 was a more intense echo group than O1. Apart from intensity the main difference between the two echo groups appears to have been size (see Fig. 9). At lower rainrates O1 was much larger than K1.

---

[2]With this correction the coldest H37 footprint shifted to a position just north of Liberal, Missouri.

Differences in the coldest infrared cloud top temperature for each echo group were small. The lowest was M1 (204 K). Coldest cloud top temperatures for K1 and O1 were within 3°C of M1.

Differences between echo groups were explored in one other way. Using the Man-computer Interactive Data Access System (McIDAS; Suomi et al., 1983), a rectangle was made which (a) was entirely contained within the digitized part of the 0047 radar rain image and (b) as nearly as possible was equivalent in area, shape and location to an echo group boundary. With overlap kept as small as possible, one such rectangle was made for each echo group. The rectangles are shown in Fig. 16.

For each rectangle a scatterplot was made of brightness temperature versus rainrate. Data were read at video (4 km) resolution. Each of the treated microwave images had been shifted to account for parallax.

All of the four plots (here O2 is treated separately from M1) show the expected cooling trend with increasing rainrate. In each of the three strongest echo groups (K1 and K2 and M1) the rate of cooling tends to diminish at intermediate and higher rain rates. Over the observed range of rainrates M1 has the largest slope. The smallest slope (roughly ½ that of M1) belongs to the echo group--K1--which in terms of peak rainrate was almost as intense as M1. This surprising result suggests that for these four echo groups size was more important than core intensity in determining the strength of the 37 GHz cold anomaly.

We also show similar scatterplots for the H18 GHz image (this, too, corrected for parallax). Differences from one echo group to the next tend to be like those observed at H37 GHz, but very much smaller. What is most remarkable about these plots is the shallowness of their slopes compared to the slopes of the H37 GHz scatterplots.

Supposing that SMMR at 37 GHz was responding to an elevated layer of ice particles, we might expect that a radar rain image taken several minutes after 0047 would more closely match patterns of brightness temperature. On the contrary, in terms of scatterplots for echo groups there is no difference of consequence in the match of 0047 and 0051 rainrates to brightness temperature. This is illustrated for echo group M1 in Fig. 19, which should be compared with Fig. 17b. Overlay comparisons of rain images with the H37 GHz image confirm this view and extend it slightly: in the present case the match suffered noticeably as soon as 8 min after the SMMR scan time.

7. Conclusions

Each of the three 37 GHz cold events observed in this case was found to be closely associated with a thunderstorm. The thunderstorms were part of a system for which the radar signature was a close conjugate of the satellite microwave signature.

The thunderstorm associated with the extreme cold event (E1) was younger and more intense than the others. It also was much larger at intermediate and high rain rates: at level-3 or higher radar reflectivity (~30 mm h^{-1} equivalent rainrate) M1 alone substantially exceeded the area of a 37 GHz SMMR footprint. Apparently it was this factor which contributed most significantly to E1's colder brightness temperature.

The cloud and echo structure of the cold event thunderstorms is consistent with the hypothesis that 37 GHz cold events are a consequence of scattering in a deep, dense ice layer. To a surprising extent in the present case rain information from SMMR was contained in the 37 GHz channels, which theory predicts ought to be most sensitive to ice. The ice

layer hypothesis also gained support from a calculation of a parallax correction for an offset observed between cold events and rain cells. On the other hand, correlations of radar rain rate and 37 GHz brightness temperature were not noticeably stronger in rain images lagged a few minutes past the time of the SMMR overpass. In fact, for lags as short as 8 min, the match was noticeably weaker.

A look at the mesoscale context of these cold events should help to establish their relationship to thermodynamic instability, the freezing level and boundary-layer forcing. Soil moisture is another factor which might fruitfully have been pursued. The biggest omission of the present study is a test of the capacity of microwave radiative transfer models to replicate the patterns of SMMR brightness temperature observed in the present case. Such work ought to be pursued, especially for cases where ground-based observations of storm structure are more complete than was true for the present case.

Acknowledgments The work described in this paper was funded by NASA Grant NAG 5-391 and by NOAA Contract NA-84-DGC-00240. I wish to thank Dr. Roy Spencer for help in getting started, Dr. Barry Hinton for help in getting finished and Mr. Michael Howland and Mrs. Hwei-Fang Chen for help in-between. Thanks also are extended to Mrs. Angela Crowell, for typing the manuscript.

7/DM10/10

Table 1. Rain areas and peak rain rates for echo groups.

Threshold ($mm\ h^{-1}$)	Echo Group	Rain Area ($km^2 \times 100$)					
		0040	0043	0047	0051	0055	0059 CST
28	01	5	3	4	2	4	3
(VIP-3)							
	K1	2	2	4	5	5	5
	K2 + M1	18	14	18	16	17	14
56	01	1	1	0	0	0	0
(VIP-4)							
	K1	0	0	1	1	0	1
	K2 + M1	5	3	5	3	2	3
Peak Rain Rate ($mm\ h^{-1}$)	01	59	59	37	37	37	32
	K1	51	51	76	68	51	68
	K2 + M1	85	68	76	68	68	68

REFERENCES

Corbell, R. P., C. J. Callahan, and W. J. Kotsch, 1979: The GOES/SMS User's Guide. National Environmental Satellite and Data Information Services, NOAA, Washington, D. C., 118 pp.

Espenshade, E. B., Jr., and J. L. Morrison (eds.), 1974: Goode's World Atlas. Rand McNally, Chicago, 372 pp.

Fraser, R. S., 1975: Interaction mechanisms--within the atomsphere. Chap. 5 in Manual of Remote Sensing, Vol. 1: Theory, Instruments and Techniques. F. J. Janza, Ed., Amer. Soc. of Photogrammetry, Falls Church, Va., 181-233.

Grody, N. C., 1984: Precipitation monitoring over land from satellites by microwave radiometry. Proceedings of IGARSS '84 Symposium (Strasbourg, 27-30 Aug 1984; Ref. ESA SP-215), 417-422.

Landsberg, H. E., 1984: Variability of the precipitation process in time and space. Sampling and Analysis of Rain, ASTM STP 823 (S. A. Campbell, Ed.), American Society for Testing and Materials, 3-9.

National Oceanic and Atmospheric Administration, 1979: Storm Data. Vol. 21, No. 6, National Climatic Center, Asheville, N. C., 30 pp.

Maddox, R. A., 1980: Mesoscale convective complexes. Bull. Am. Meteor. Soc., 61, 1374-1387.

Njoku, E. G., J. M. Stacey and F. T. Barath, 1980: The Seasat Scanning Multichannel Microwave Radiometer (SMMR): Instrument description and performance. IEEE J. Oceanic Enrg., OE-5, 100-115.

Savage, R. C., 1976: The Transfer of Thermal Microwaves through Hydrometeors. Ph.D. thesis, Dept. of Meteorology, University of Wisconsin, Madison, 147 pp.

Spencer, R. W., 1984: Satellite passive microwave rain rate measurement over croplands during spring, summer and fall. J. Clim. Appl. Meteor., 23, 1553-1562.

Spencer, R. W., and N. C. Grody, 1985: The measurement of precipitation over land and ocean with satellite microwave radiometers--techniques and opportunities. Submitted to Bull. Amer. Meteor. Soc.

Spencer, R. W., M. R. Howland and D. Santek, 1985: Severe storm detection with satellite passive microwave radiometery. To be submitted to J. Clim. Appl. Meteor.

Spencer, R. W., W. Olson, R. Wu, D. W. Martin and J. A. Weinman, 1983: Heavy thunderstorms observed over land by the Nimbus 7 Scanning Multichannel Microwave Radiometer. J. Clim. Appl. Meteor., 22, 1041-1046.

Suomi, V. E., R. Fox, S. S. Limaye and W. L. Smith, 1983: McIDAS III: A modern interactive data access and analysis system. J. Appl. Meteor., 22, 766-778.

Wu, R., and J. A. Weinman, 1984: Microwave radiances from precipitating clouds containing aspherical ice, combined phase, and liquid hydrometeors. J. Geophys. Res., 89 (No. D5), 7170-7178.

Captions

1. Scanning Multichannel Microwave Radiometer images at 0047 on 23 June 1979. Clockwise from the upper left, the states shown are Kansas, Missouri, Arkansas and Oklahoma. The central cross marks the position of the Monett, MO National Weather Service WSR-57 radar. Each arm of the angle in the lower right corner is 100 km in length.
   a. 37 GHz horizontal polarization.
   b. 37 GHz vertical polarization.
   c. 21 GHz horizontal polarization.
   d. 21 GHz vertical polarization.
   e. 18 GHz horizontal polarization.
   f. 18 GHz vertical polarization.
   g. 10.6 GHz horizontal polarization.
   h. 10.6 GHz vertical polarization.
   i. 6.6 GHz horizontal polarization.
   j. 6.6 GHz vertical polarization.

2. Maps of SMMR 37 GHz brightness temperature (K) for 0047. Except as noted contours are at intervals of 10°C. Stippling indicates temperatures warmer than 260 K. A cross marks the location of Liberal, MO; a circled cross the location of the Monett radar.
   a. Horizontal polarization.
   b. Vertical polarization.

3. SMMR images of polarization temperature difference (V-H, with large positive differences indicated by lighter tones). Otherwise, as for Fig. 1.

   a. 37 GHz.

   b. 18 GHz.

   c. 10.6 GHz.

   d. 6.6 GHz.

4. Map of 37 GHz polarization temperature difference. The interval between contours is 5°C. Values of δT_b greater than 15°C are stippled and the 10°C contour is shown by the heavy line. Otherwise as for Fig. 2.

5. Part of the National Weather Service radar summary chart for 0035 on 23 June. Contours are at echo intensities of 1, 3 and 5. Reported echo top heights are indicated by dots. Adjacent underlined numbers give radar-measured echo top heights, in thousands of feet. Also shown are movements of the comma echo and of one or more cells in the comma echo by, respectively, the pennant (30 kn) and the arrow (30 kn). Three small rectangles within the comma echo give the positions of the coldest footprints in each of the three cold events E1, E2 and E3. Copied information is complete only for the comma echo.

6. Map of echo group boundaries composited over the interval 0019 through 0059. Echo groups are labelled. A cross marks the location of the Monett radar and an ellipse of dots indicates the 220 km range circle.

7. Map of gauge rainfall, NWS cooperative network, for the hour ending at 0100 on 23 June. Units are millimeters. The outermost contour corresponds to 0.25 mm. Gauge locations are marked by dots. The location of the Monett radar is marked by a circled cross and the location of Liberal by a plain cross.

8. Image of radar rainfall averaged over the interval 0019 to 0059.

9. Image of radar rainfall for 0047.

10. Histogram of differences in hourly rain rates. Note the break in the scale for frequency.

11. Scatterplot of gauge and radar rainrates for the data shown in Fig. 10. Single data points are indicated by dots; double points by circles. There are 39 points at (0,0). Also shown is the line of radar rainrate regressed on gauge rainrate. Units are millimeters.

12. GOES-East infrared image for 0030 on 23 June. A location correction for perspective has been applied to this image. The cross marks the location of the Monett radar in relation to the perspective-corrected image.

13. Same as Fig. 12, except enhanced by the MB curve.

14. One-half hourly sequence of MB-enhanced infrared images.

15. Image of H37 GHz brightness temperature at 0047. Echo group boundaries at that same time are plotted over the SMMR image. Also shown for each of the strong echo groups is the location of the radar rain image peak rainrate at 0047. Axes of heavier rain are indicated by dashed lines.

16. Image of H37 GHz brightness temperature with echo group rectangles. A parallax correction has been applied to the microwave image.

17. Scatterplots of H37 brightness temperature versus radar rainrate, both at 0047, for each of the four rectangles shown in Fig. 16. Echo groups corresponding to the rectangles are indicated in the upper right corner of each scatterplot. The number below the echo group name gives the total number of data points contained in the corresponding rectangle. In each case most of these points are not individually seen because of overplotting.
    a. Box 1 in Fig. 16, corresponding to echo group K1.
    b. Box 2, corresponding to M1.
    c. Box 3, corresponding to K2 and 02.
    d. Box 4, corresponding to 01.

18. As for Fig. 17, except H18.

19. As for Fig. 17b, except in comparison with 0051 radar rainrates.

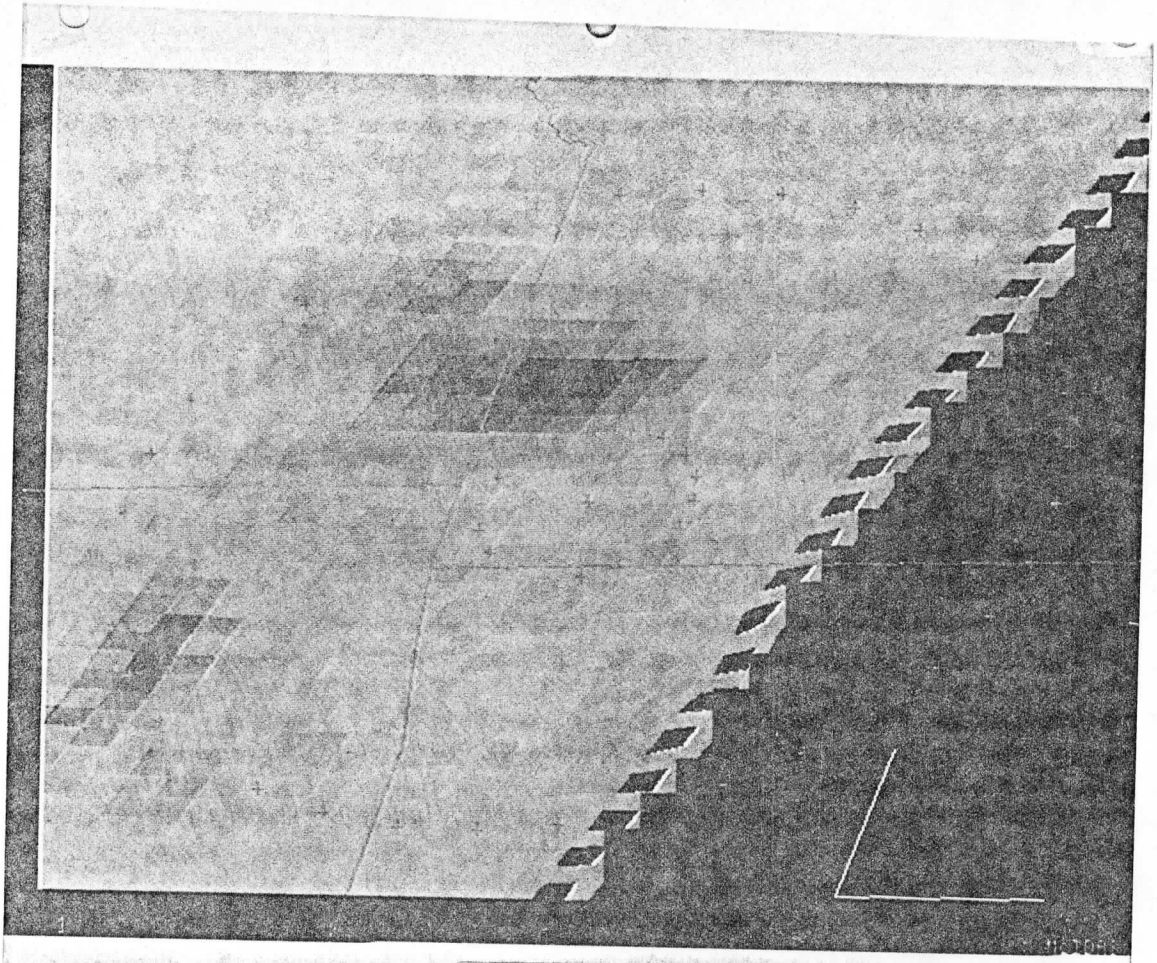

Fig. 1a

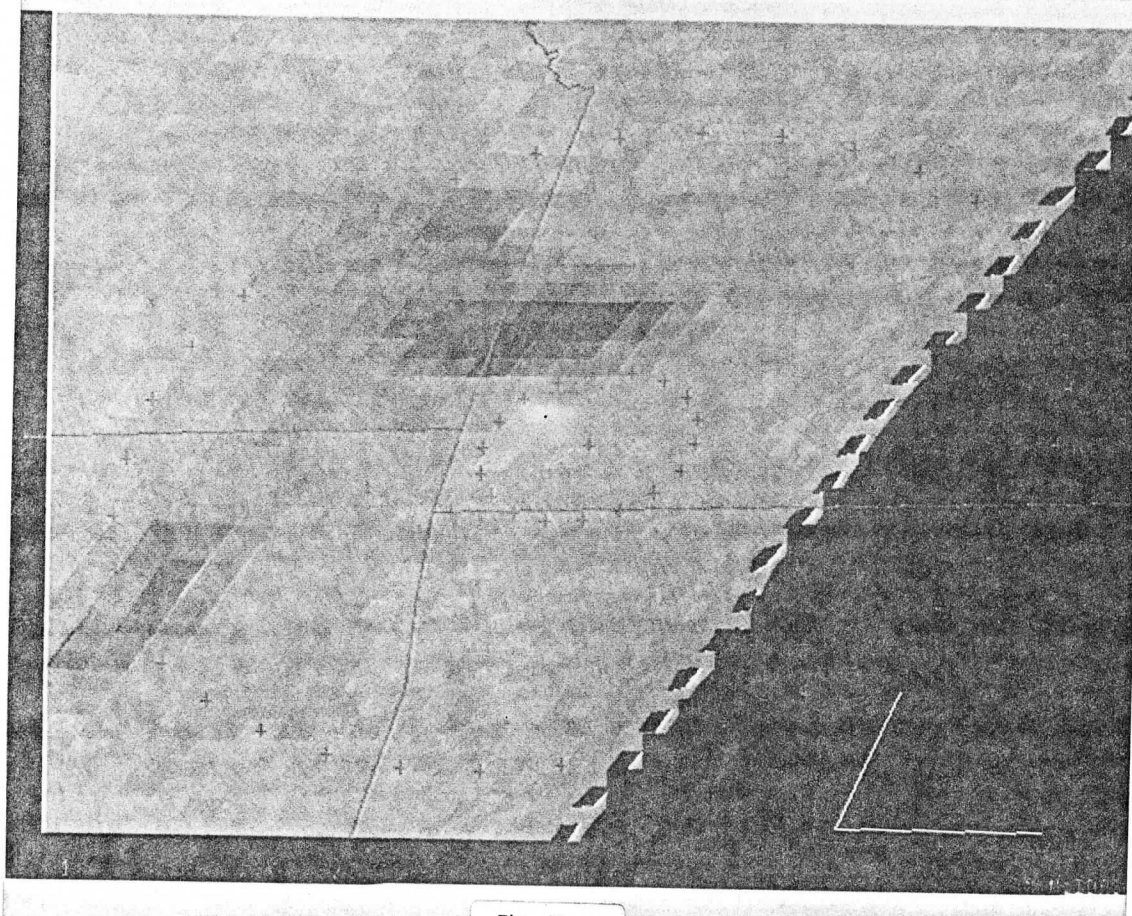

Fig. 1b

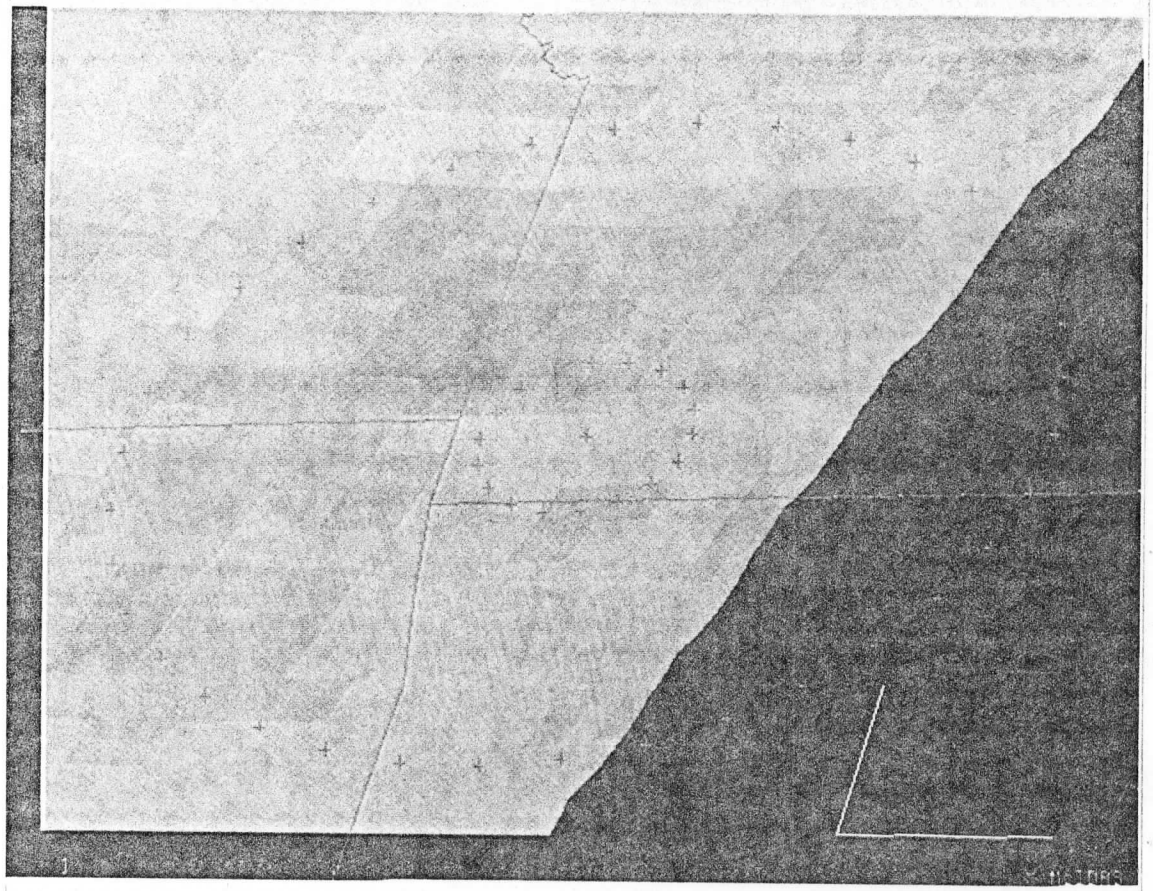

Fig. 1c

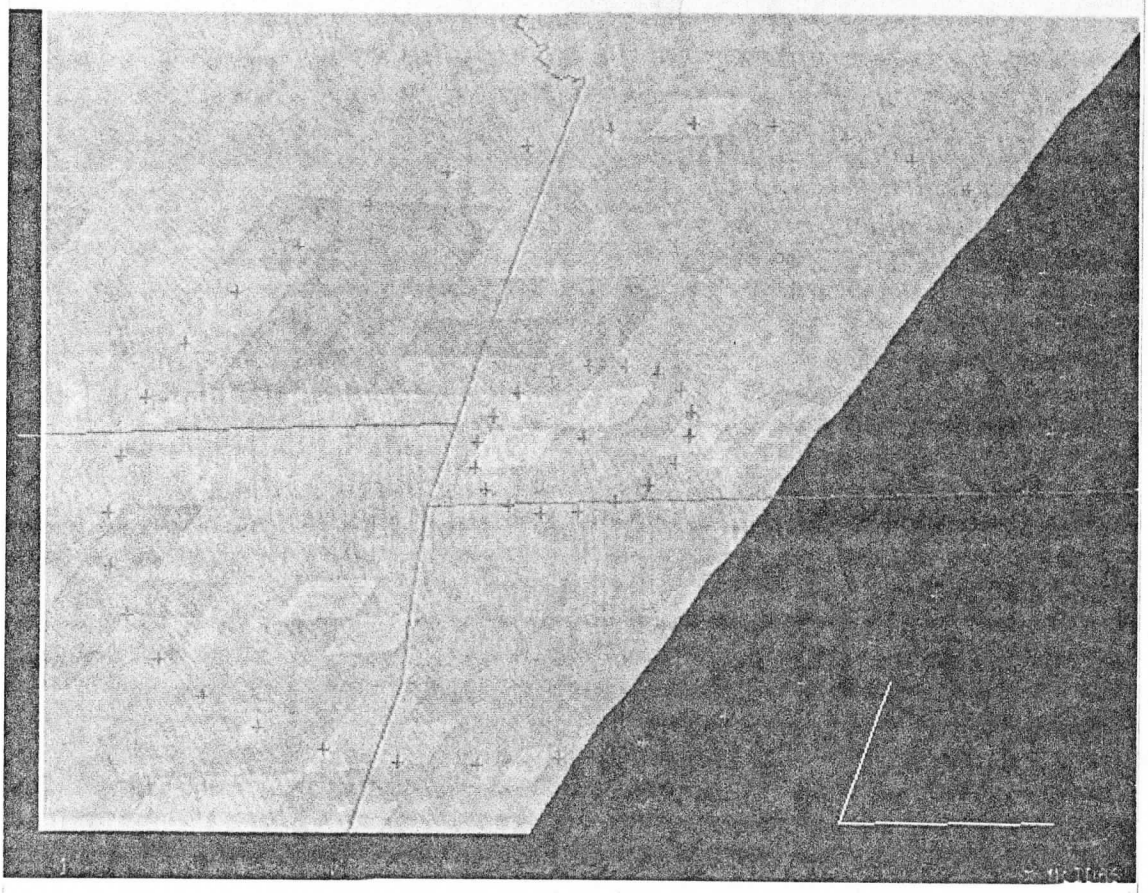

Fig. 1d

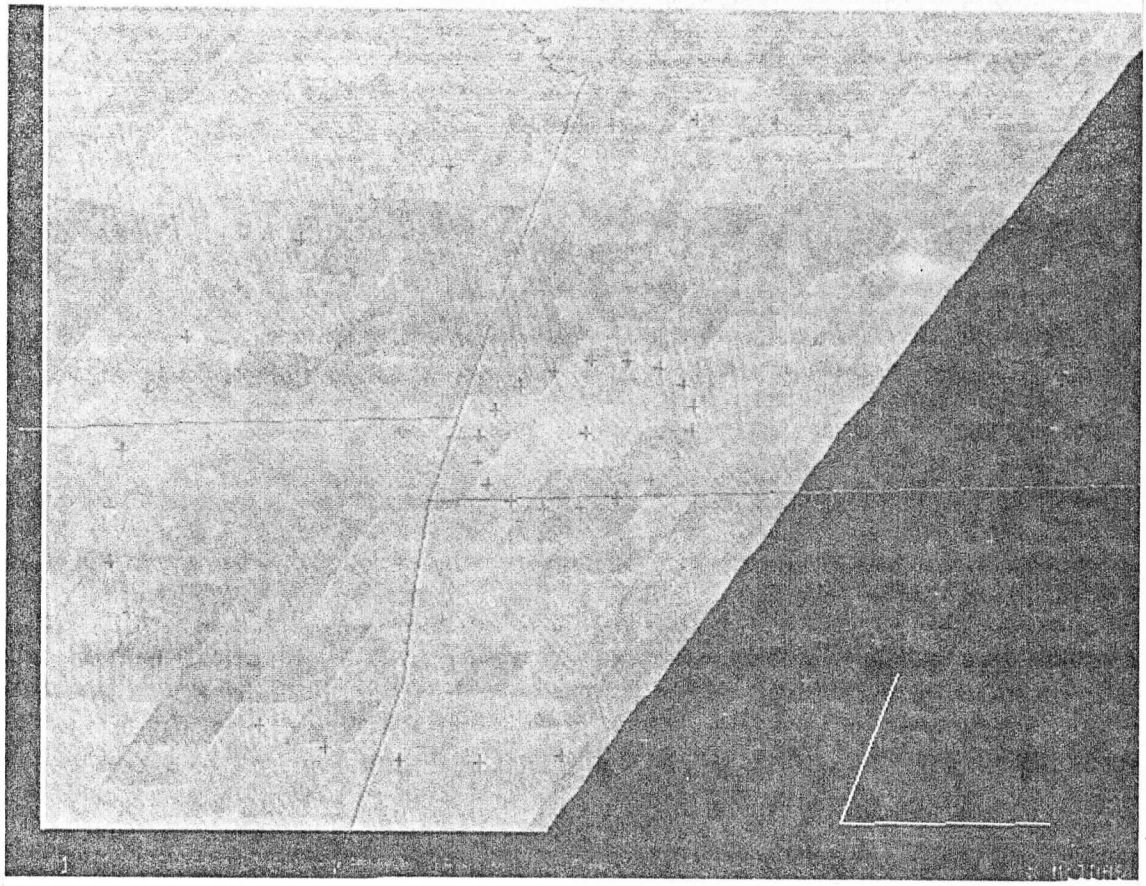

Fig. 1e

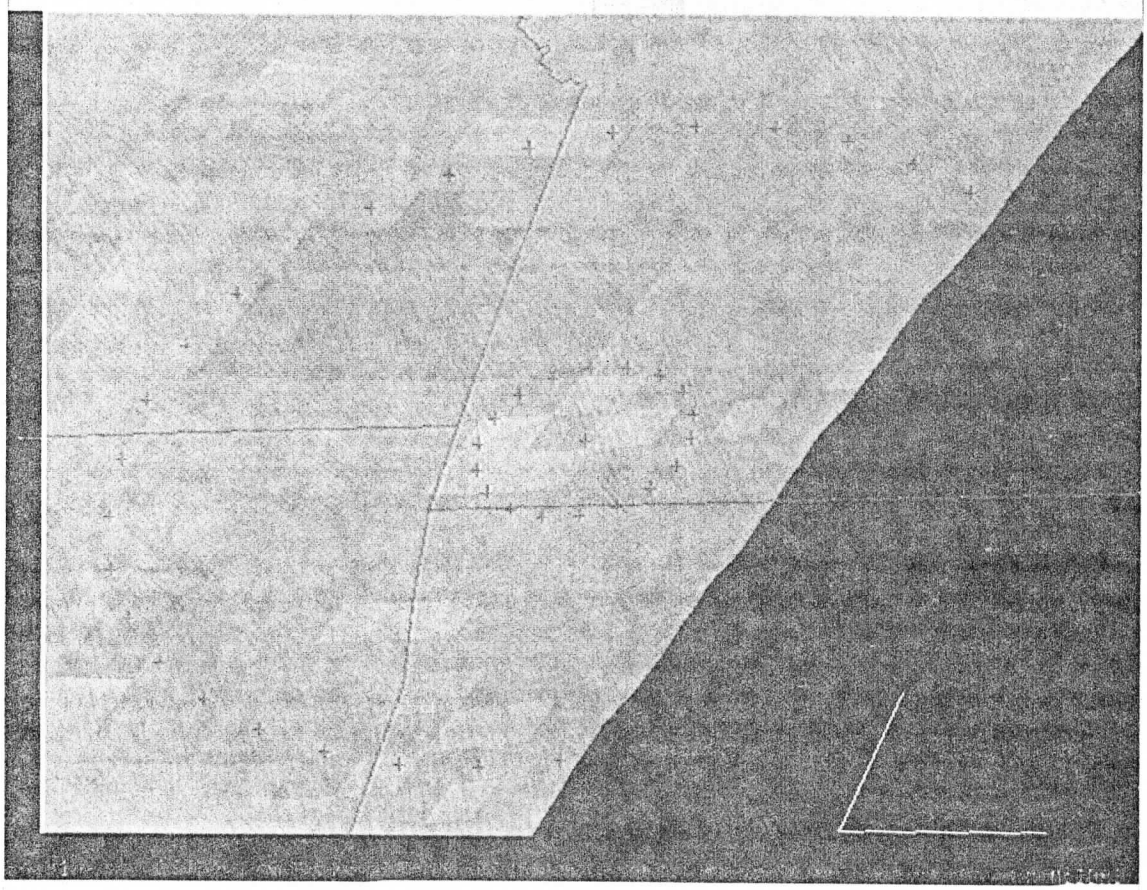

Fig. 1f

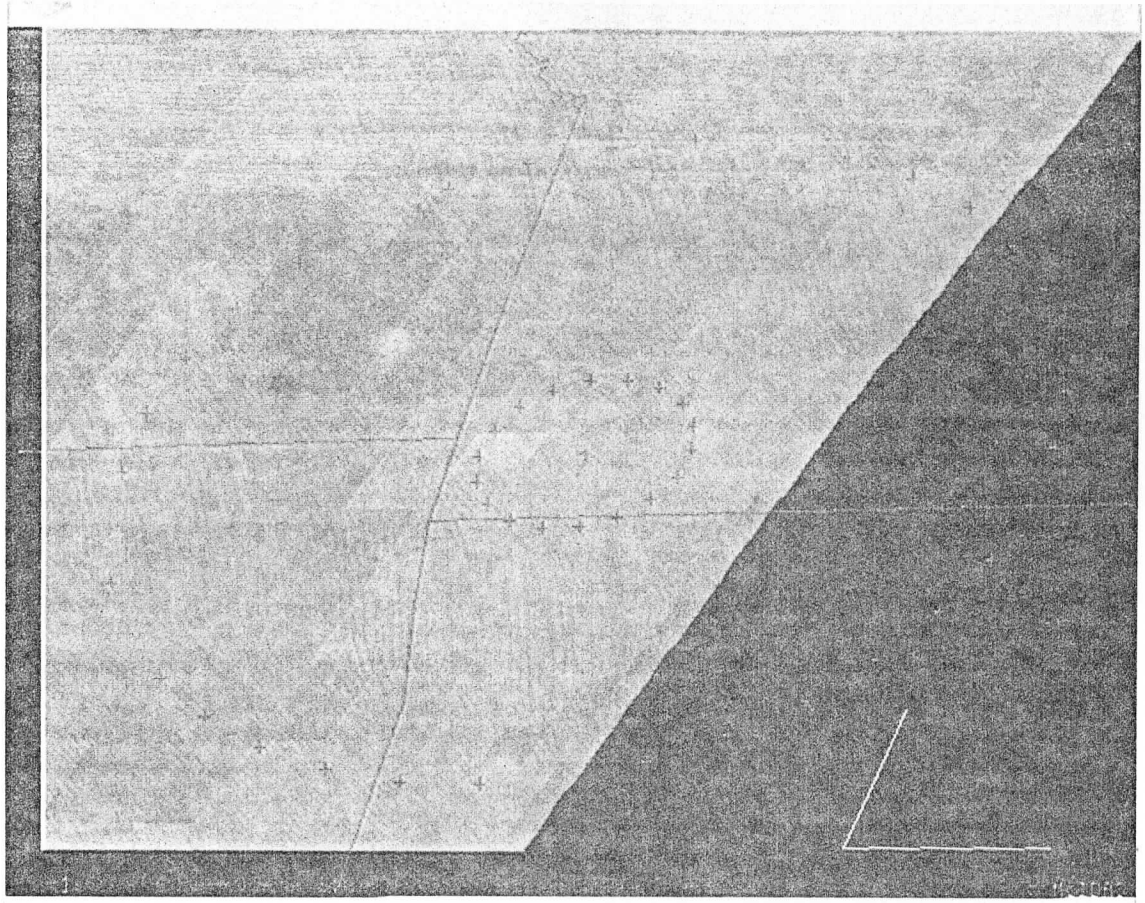

Fig. 1g

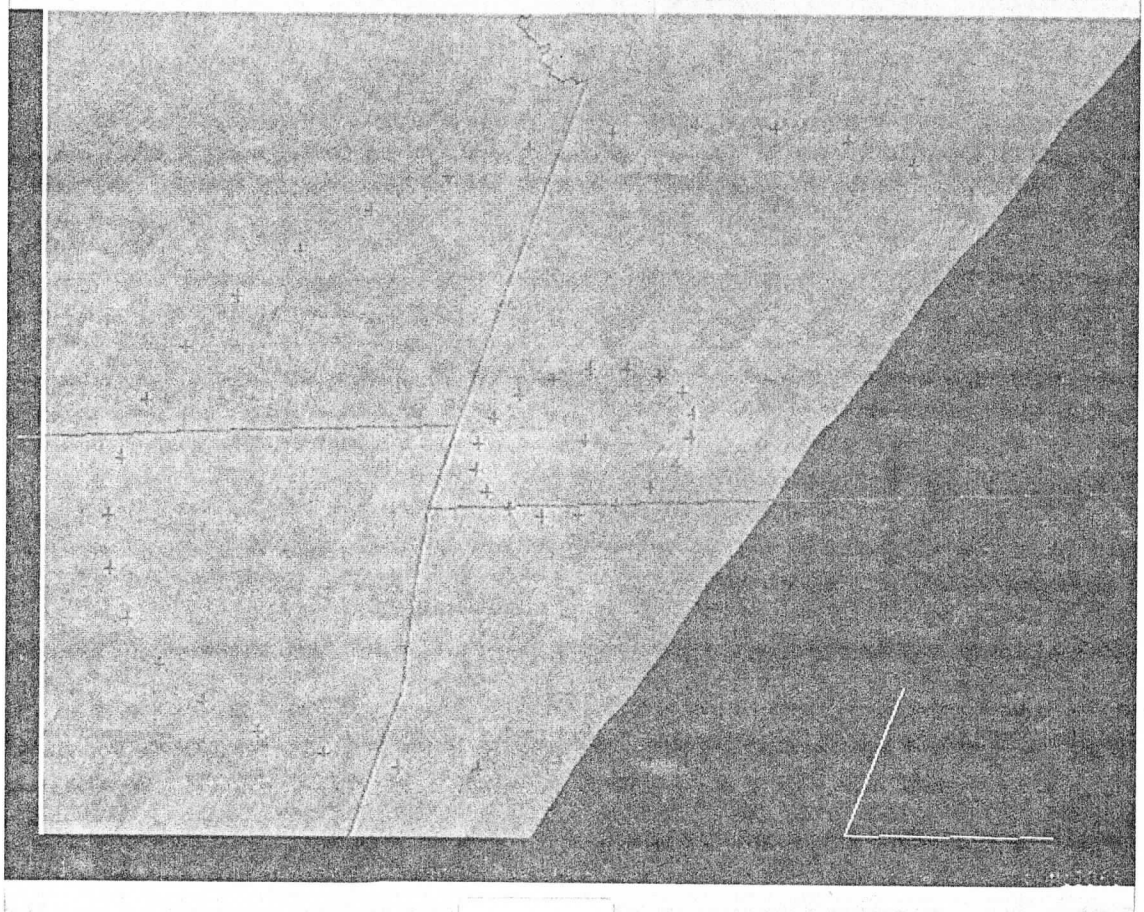

Fig. 1h

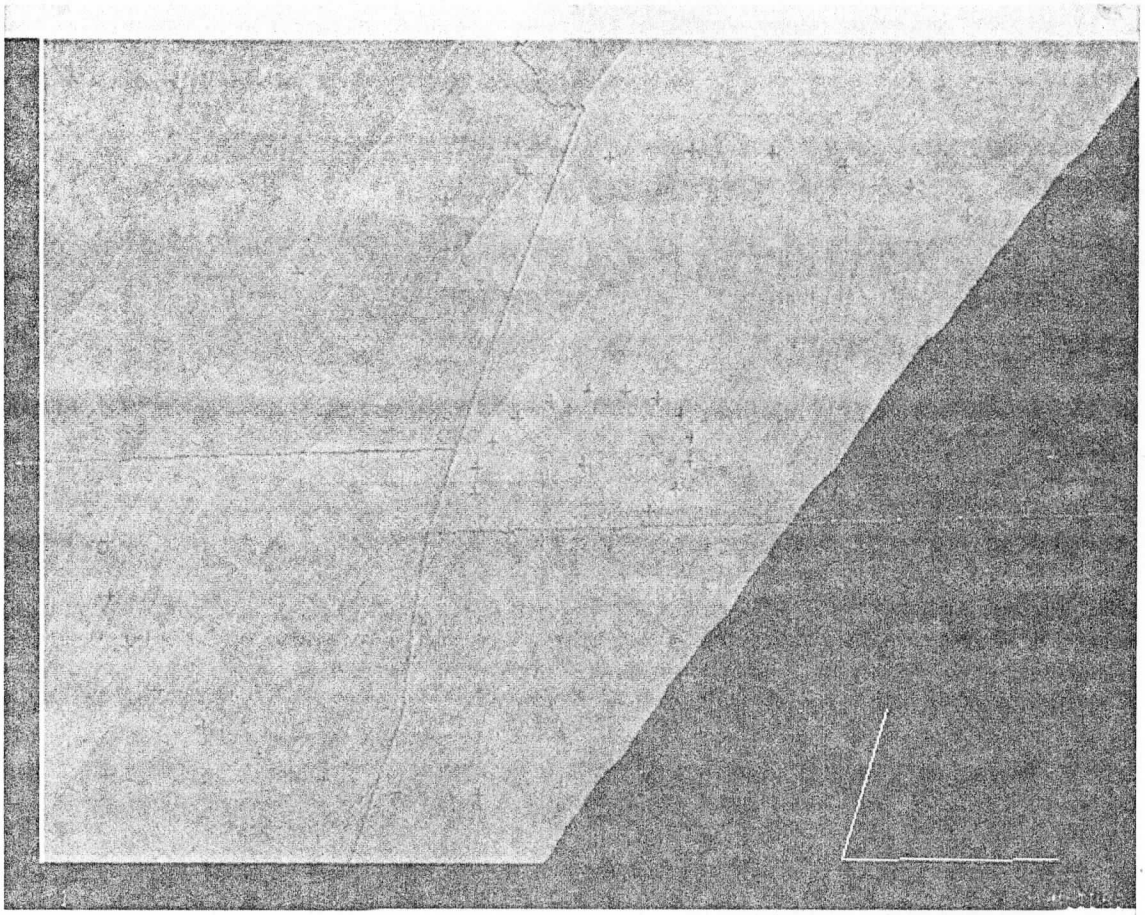

Fig. 1i

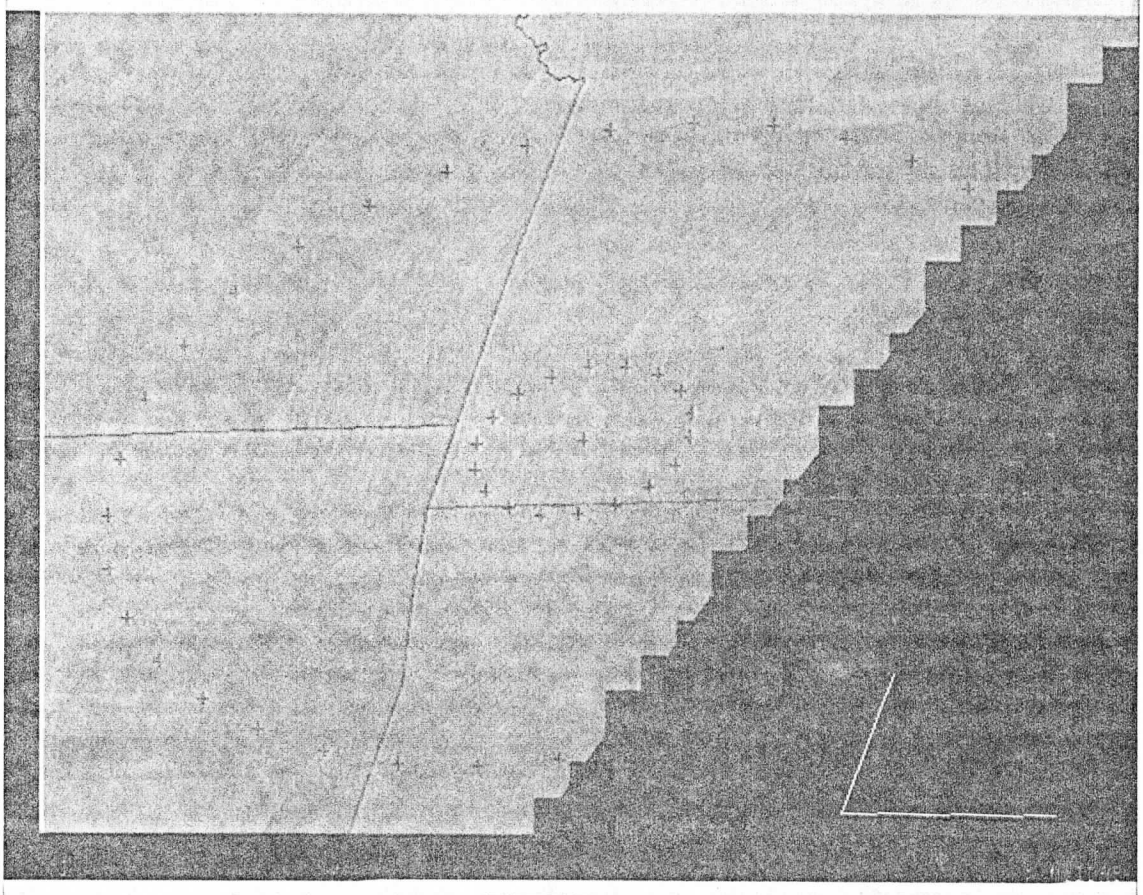

Fig. 1j

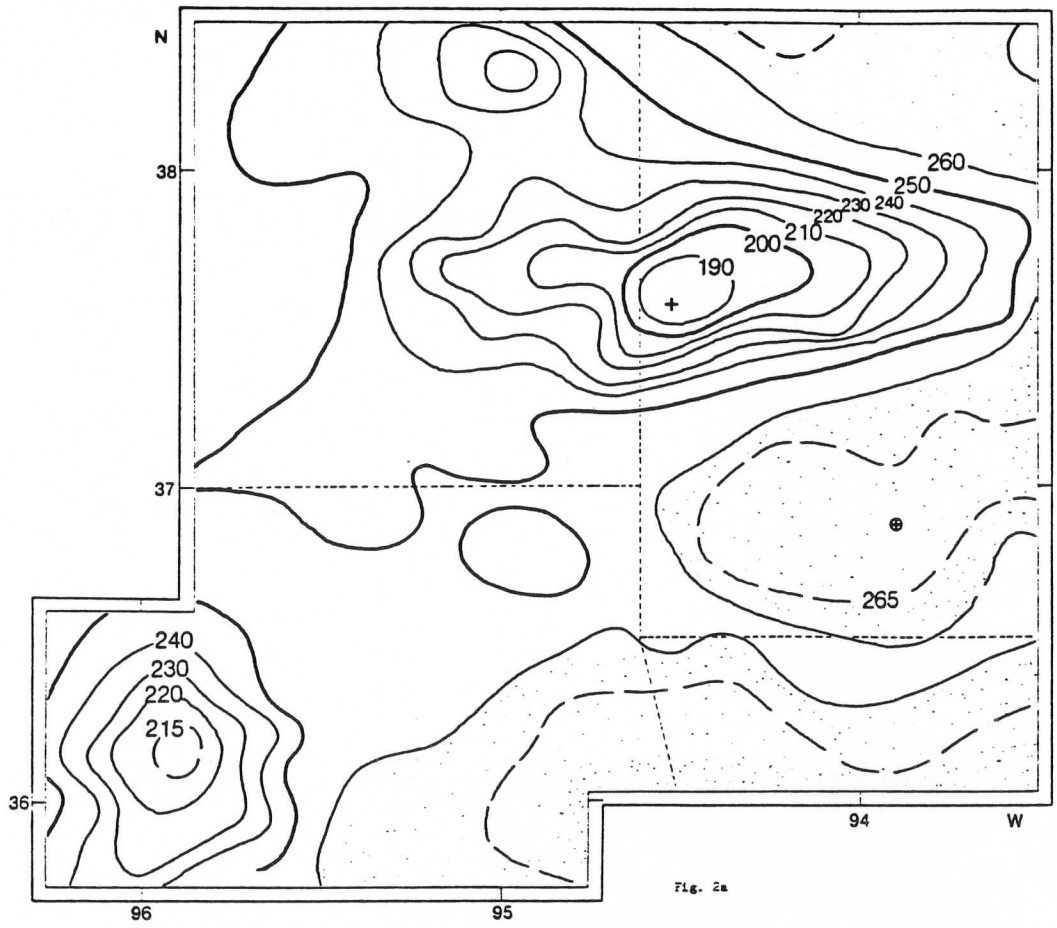
N
38
37
36
96
95
94
W
260
250
240
230
220
210
200
190
265
240
230
220
215

Fig. 2a

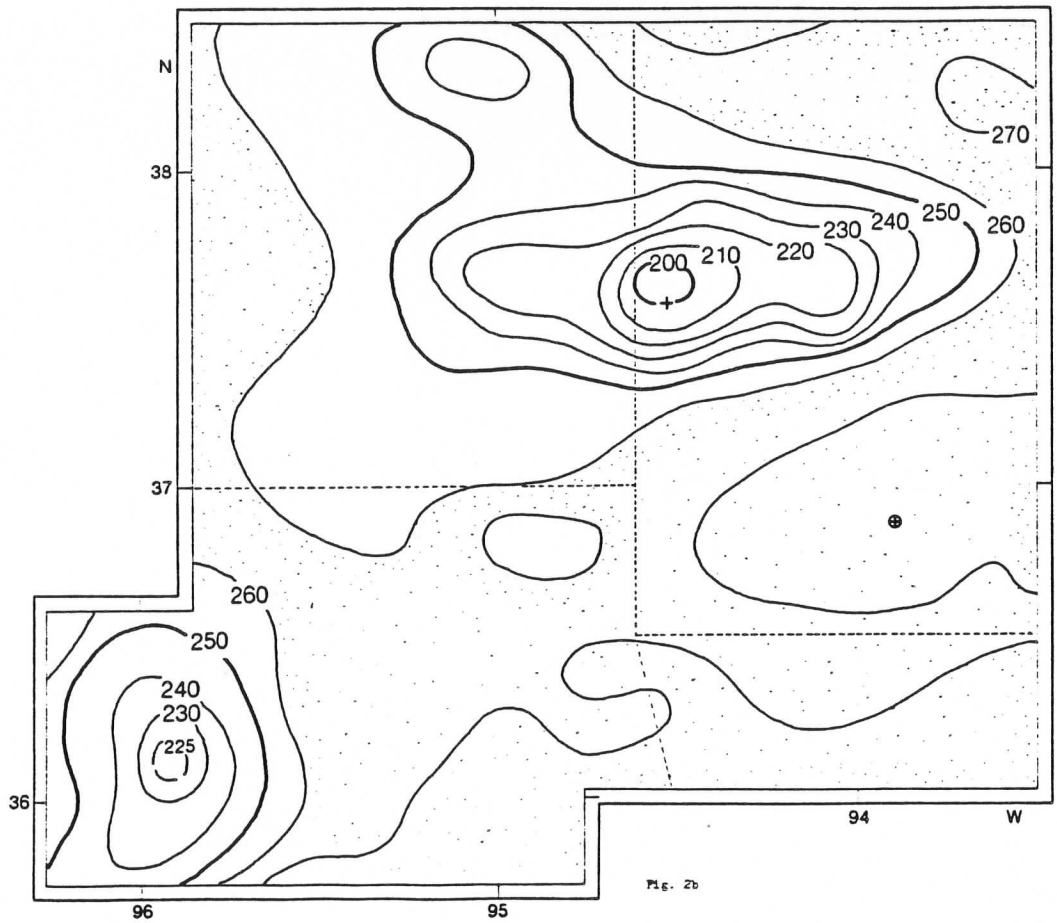
N
38
37
36
96
95
94
W
270
260
250
240
230
220
210
200
260
250
240
230
225

Fig. 2b

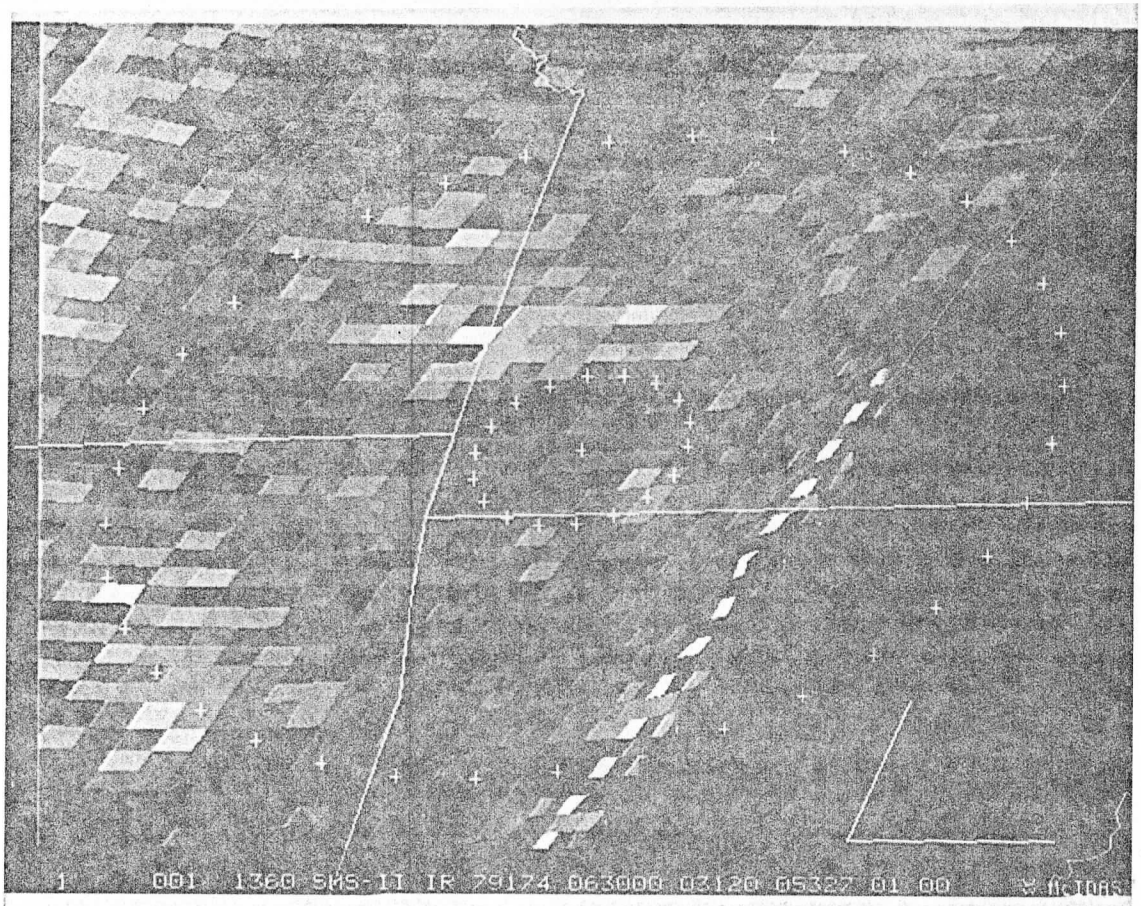
1 001 1360 SMS-II IR 79174 063000 03120 05327 01 00

Fig. 3a


1 002 1360 SMS-II IR 79174 063000 03120 05327 01 00

Fig. 3b

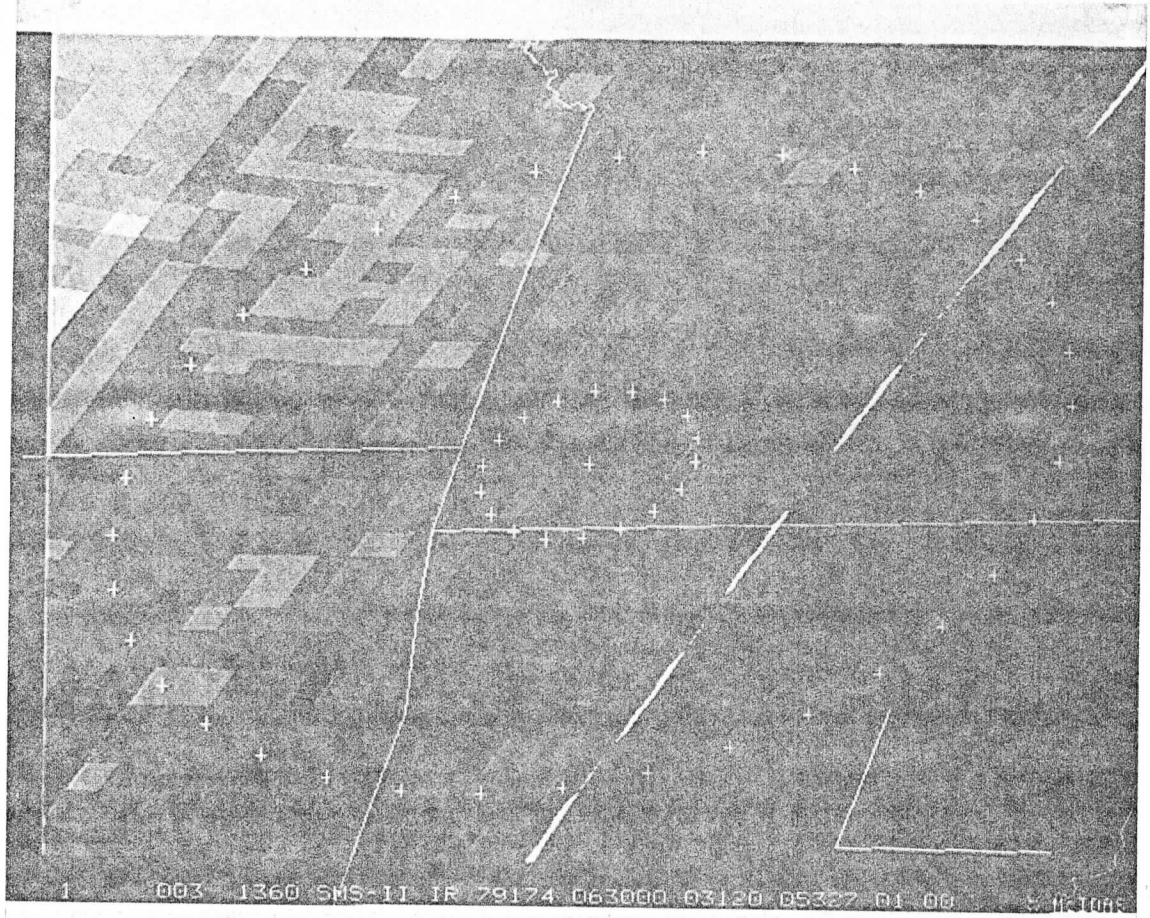
1 003 1360 SMS-II IR 79174 063000 03120 05327 01 00

Fig. 3c

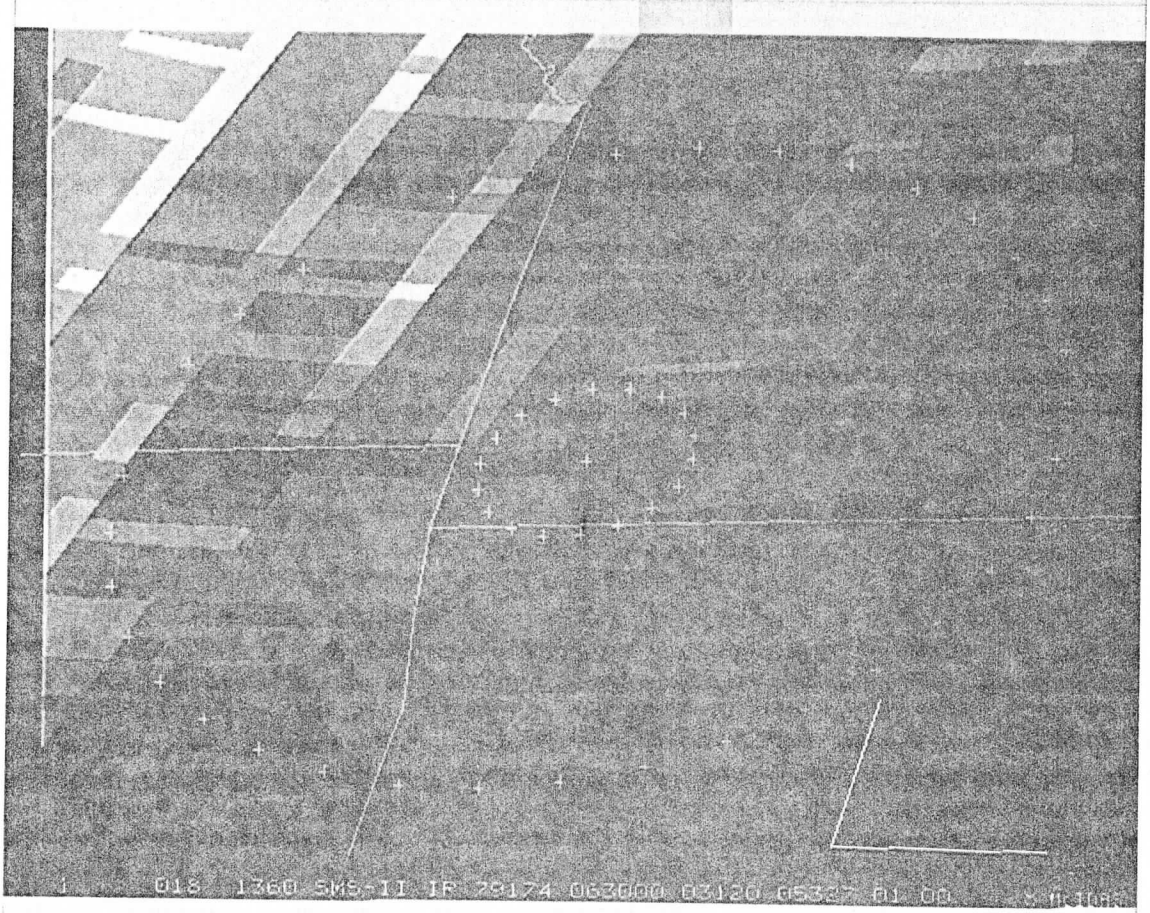
1 018 1360 SMS-II IR 79174 063000 03120 05327 01 00

Fig. 3d

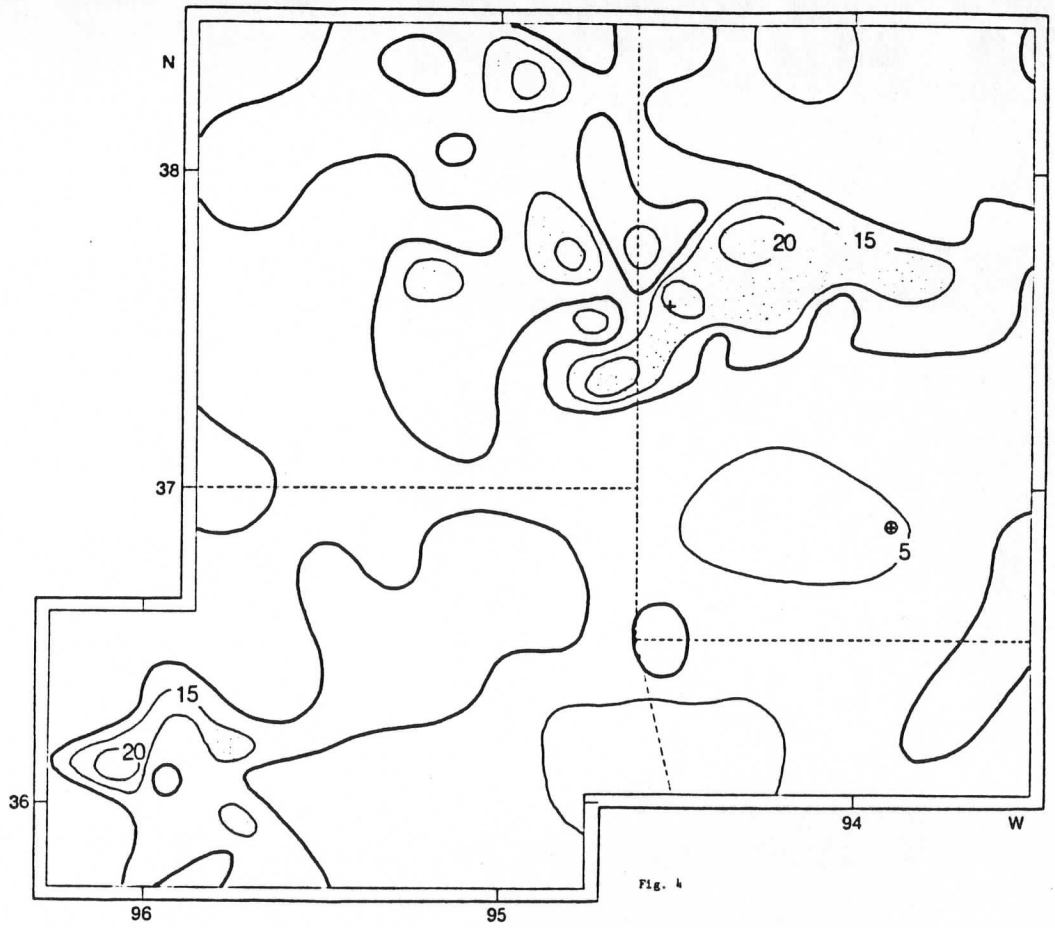
N
38
37
36
96
95
94
W
20
15
5
15
20

Fig. 4

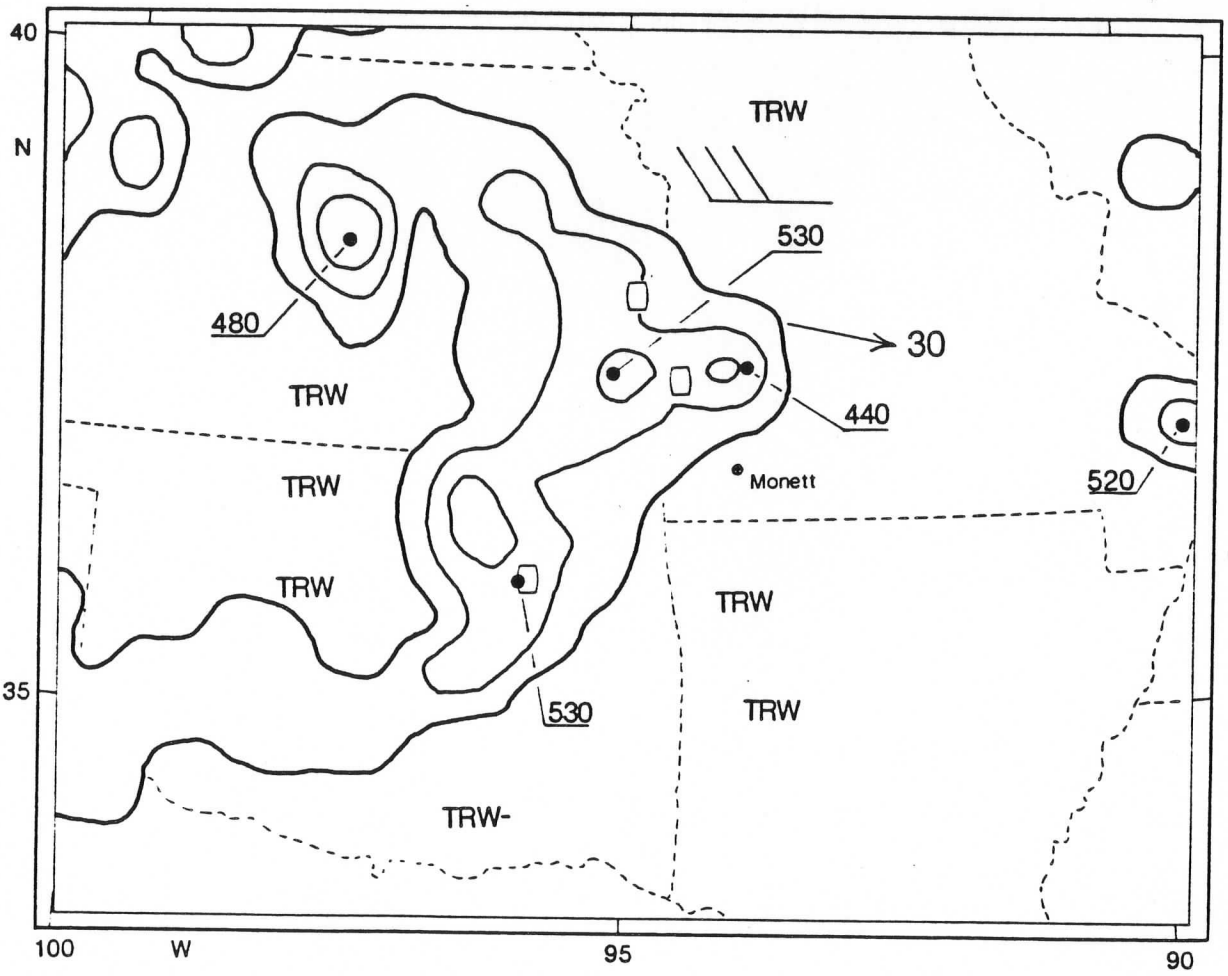
40
N
35
100
W
95
90
TRW
530
480
30
TRW
440
TRW
Monett
520
TRW
TRW
530
TRW
TRW-

Fig. 5

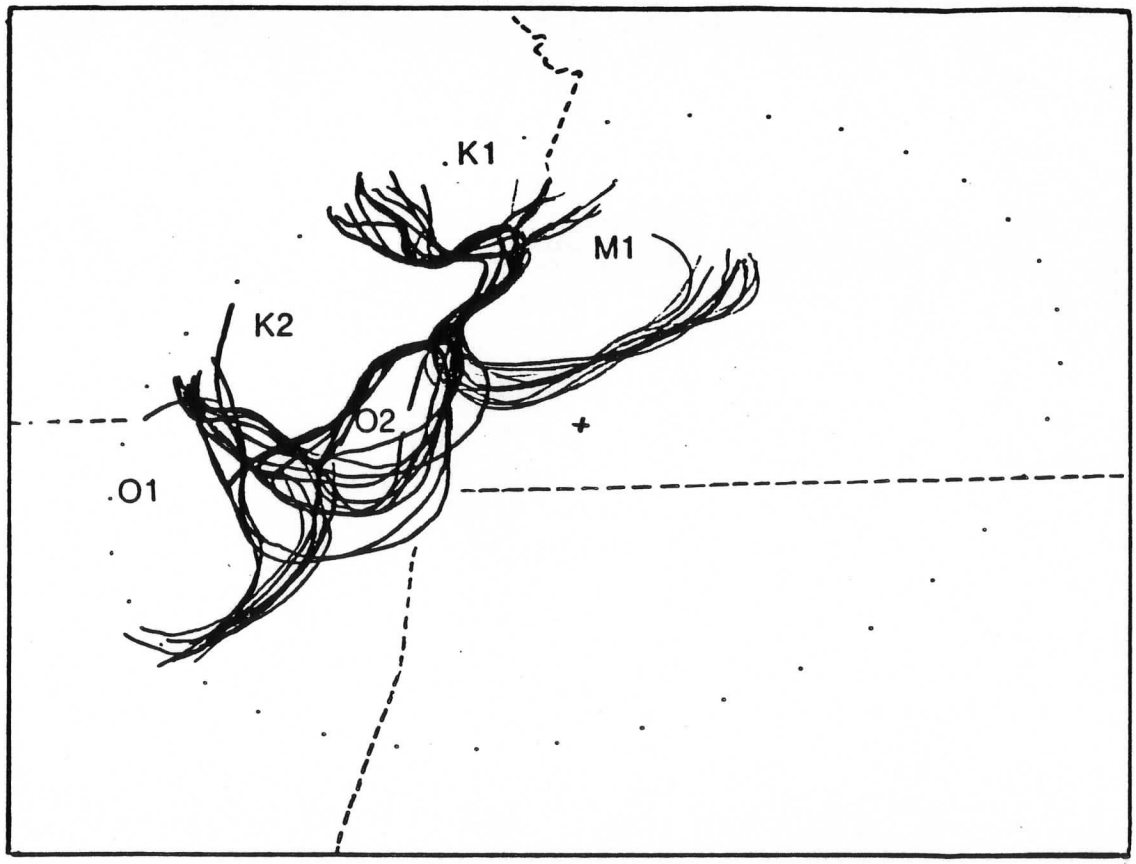

Fig. 6

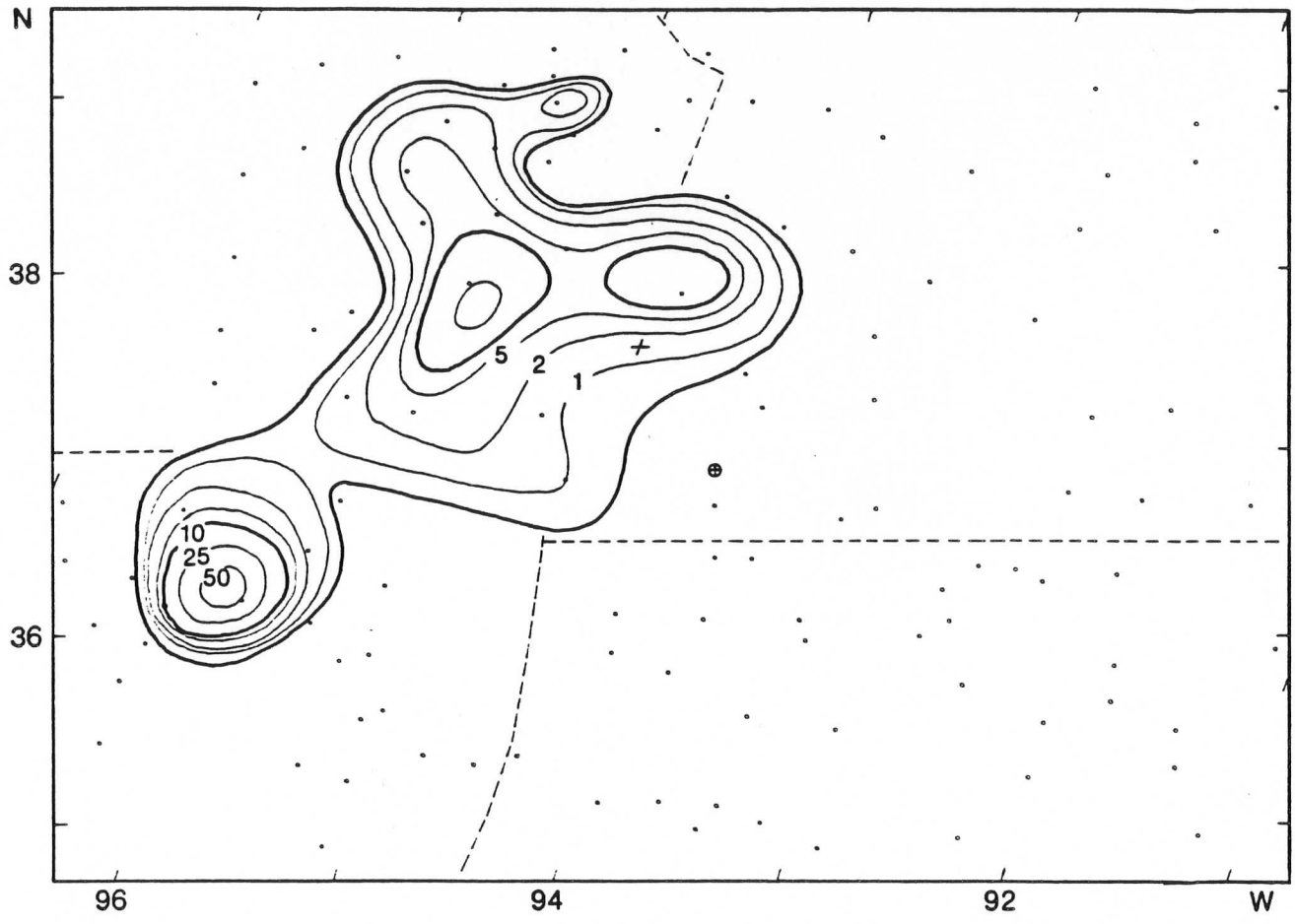

Fig. 7

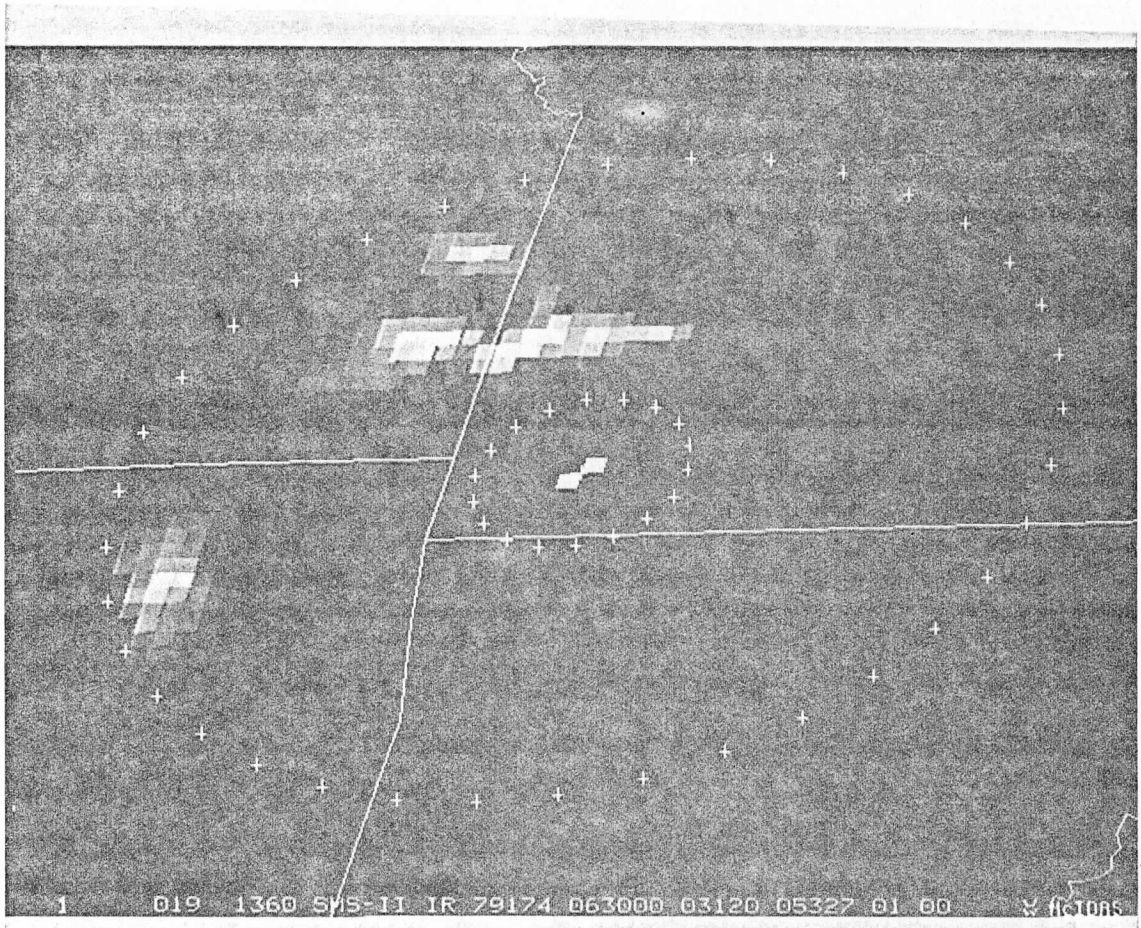

Fig. 8

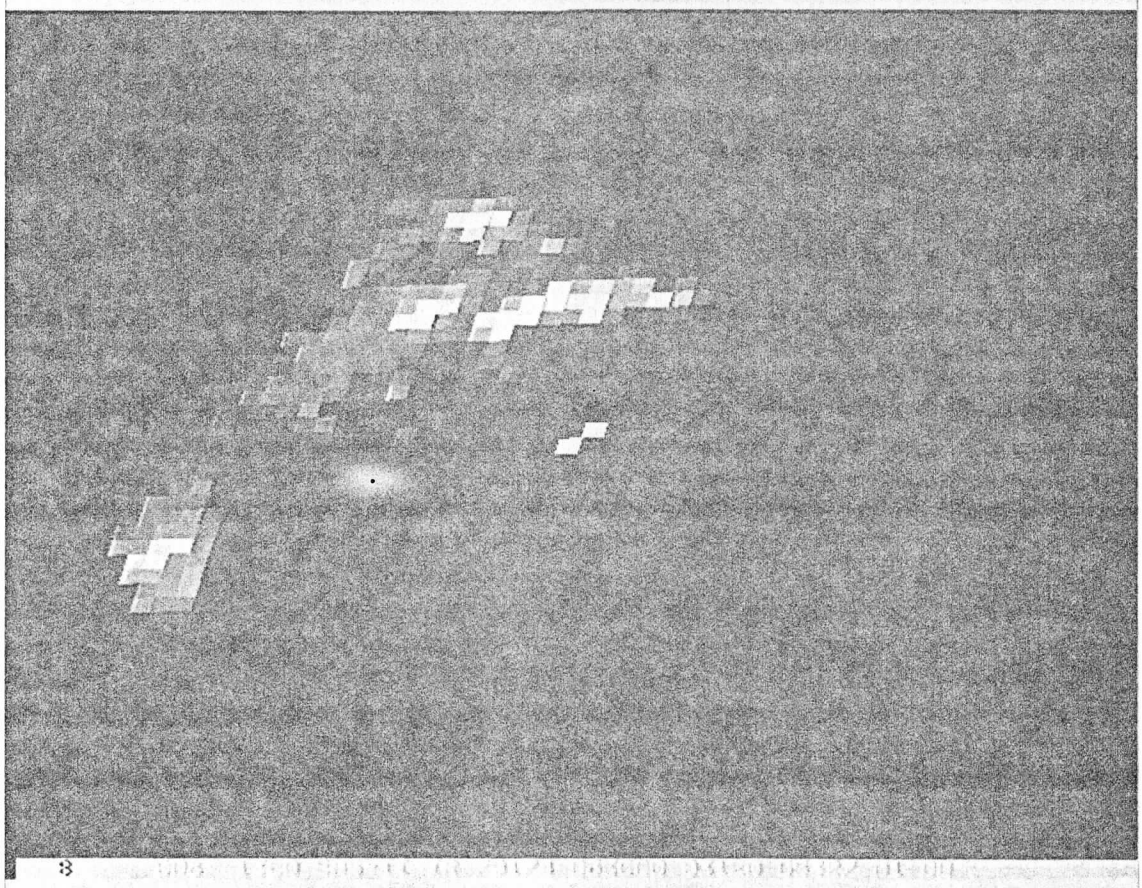

Fig. 9

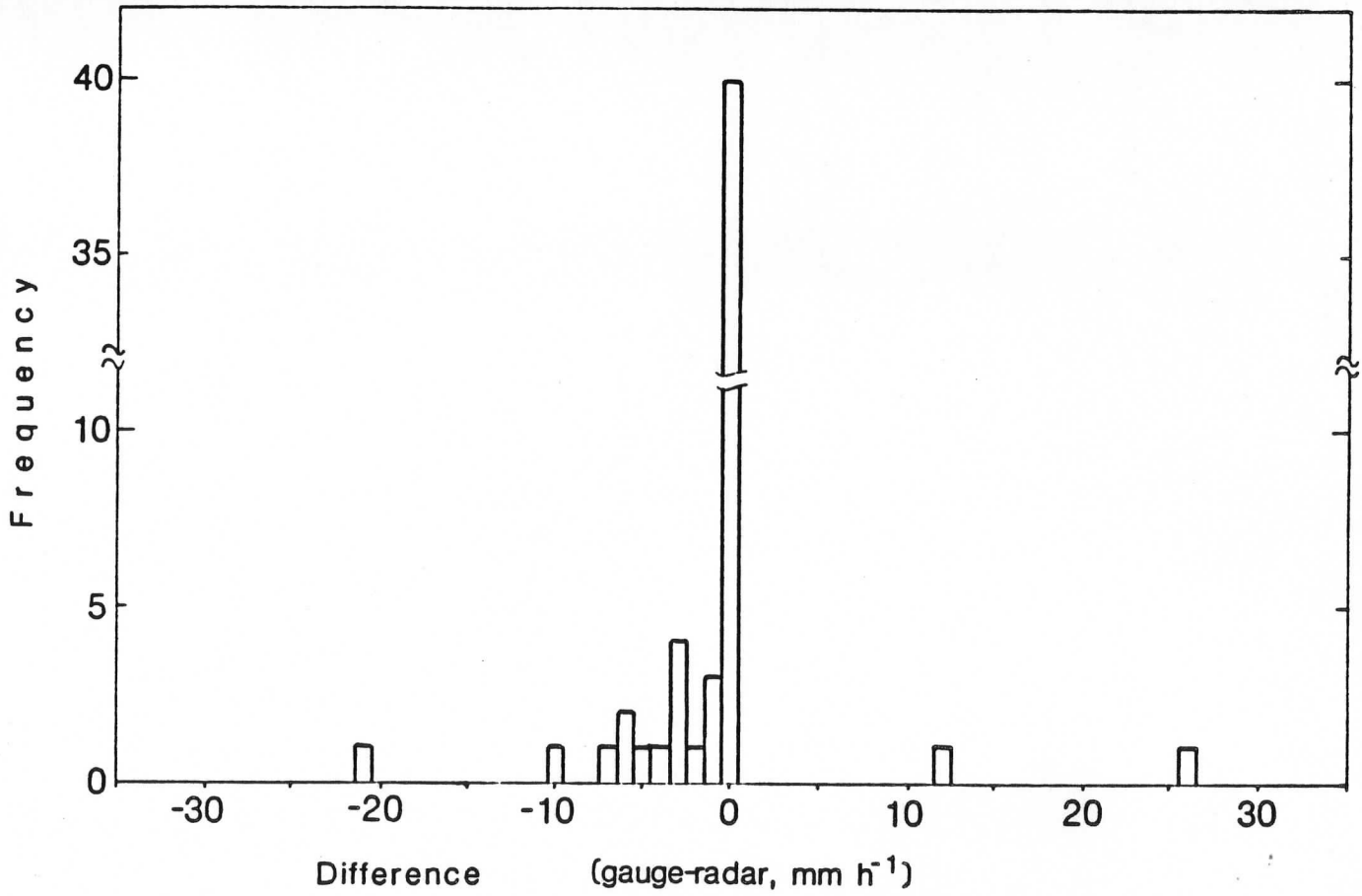
Frequency
40
35
10
5
0
-30
-20
-10
0
10
20
30
Difference (gauge-radar, mm h^{-1})

Fig. 10

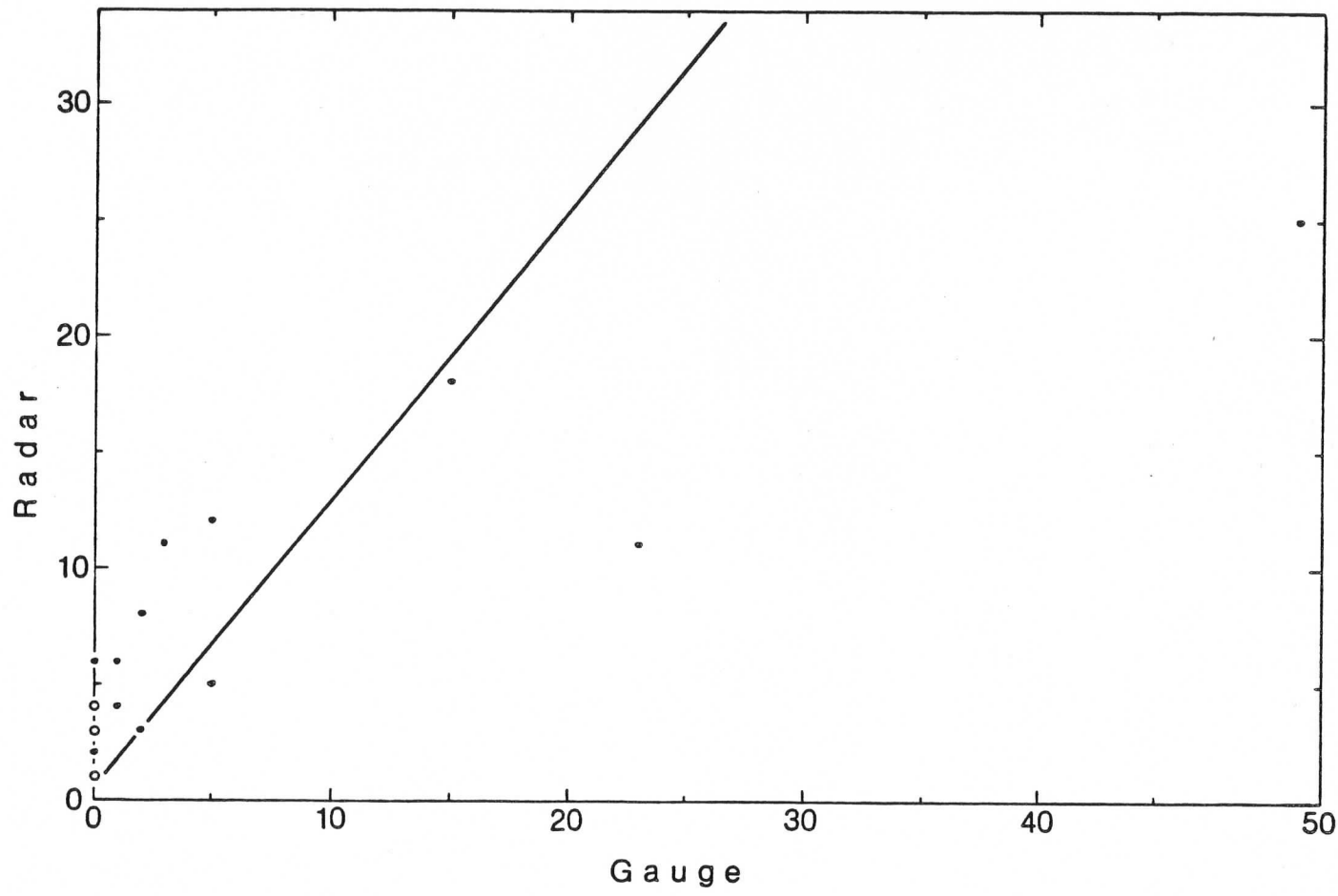
Radar
30
20
10
0
0
10
20
30
40
50
Gauge

Fig. 11

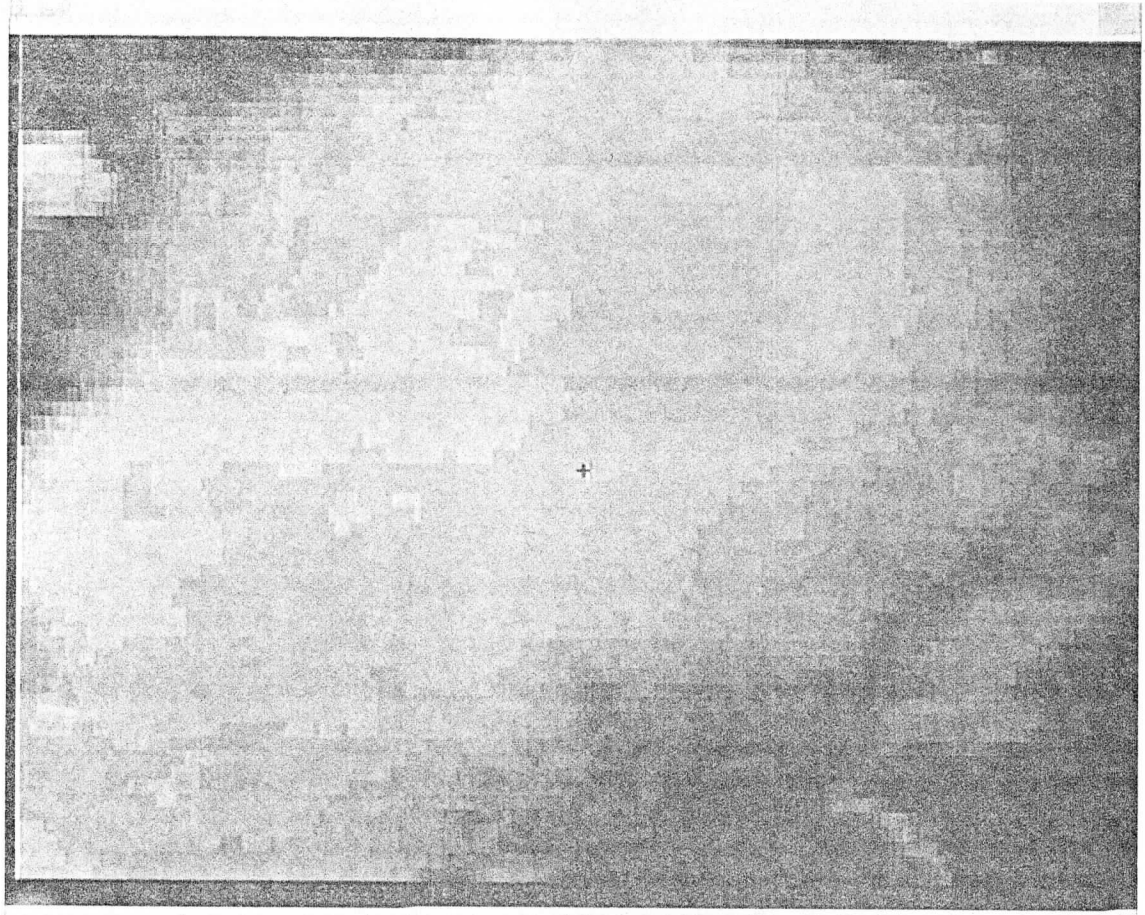

Fig. 12

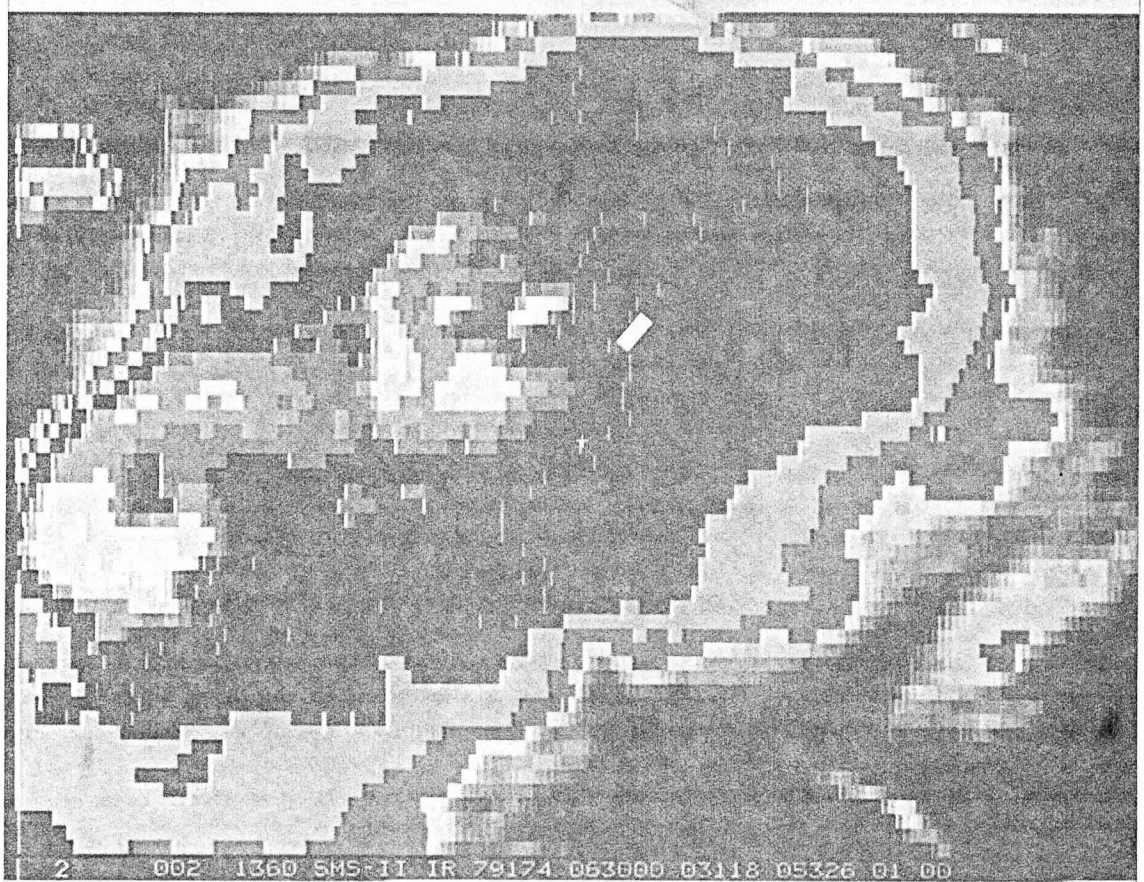

Fig. 13

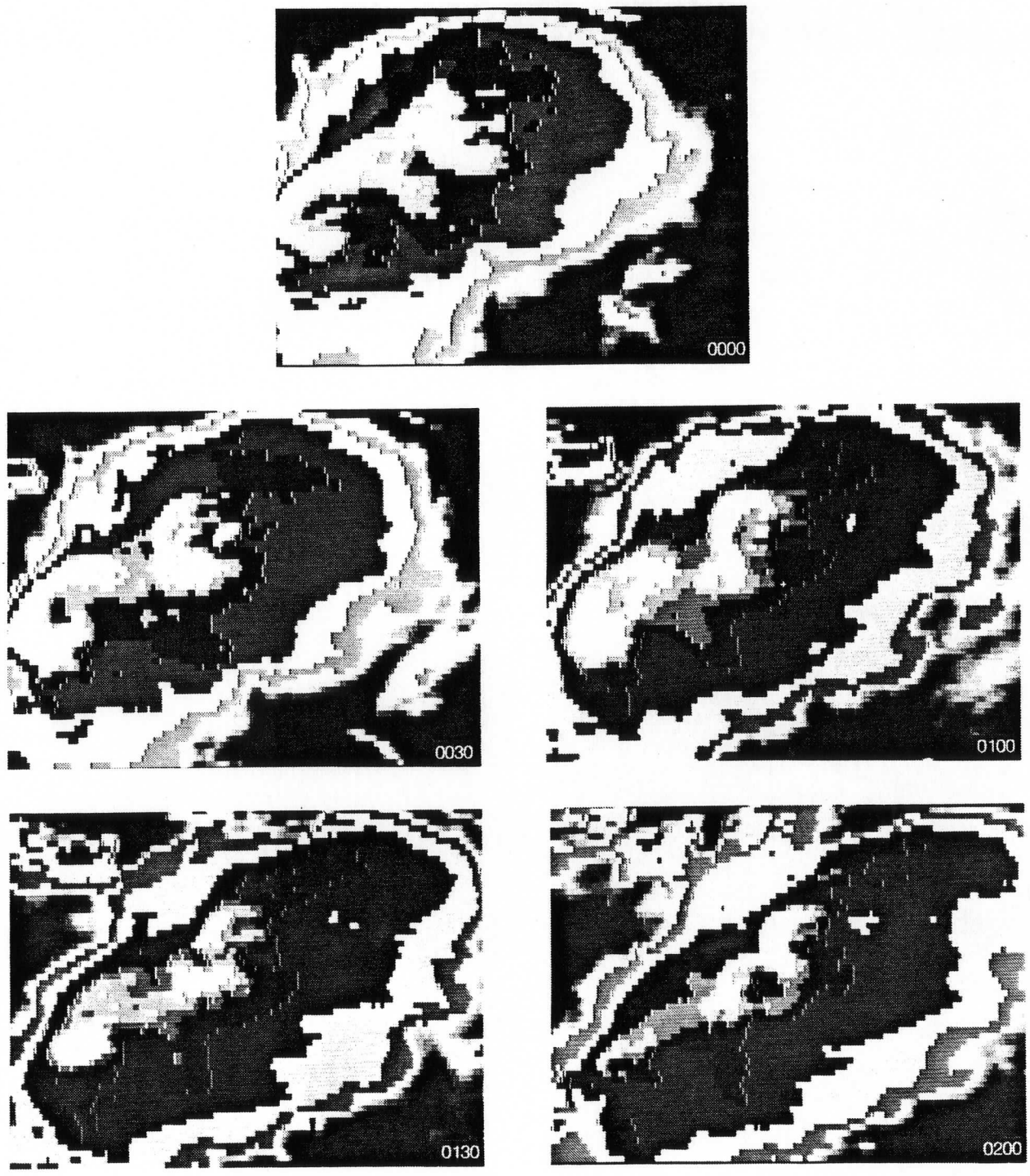

Fig. 14

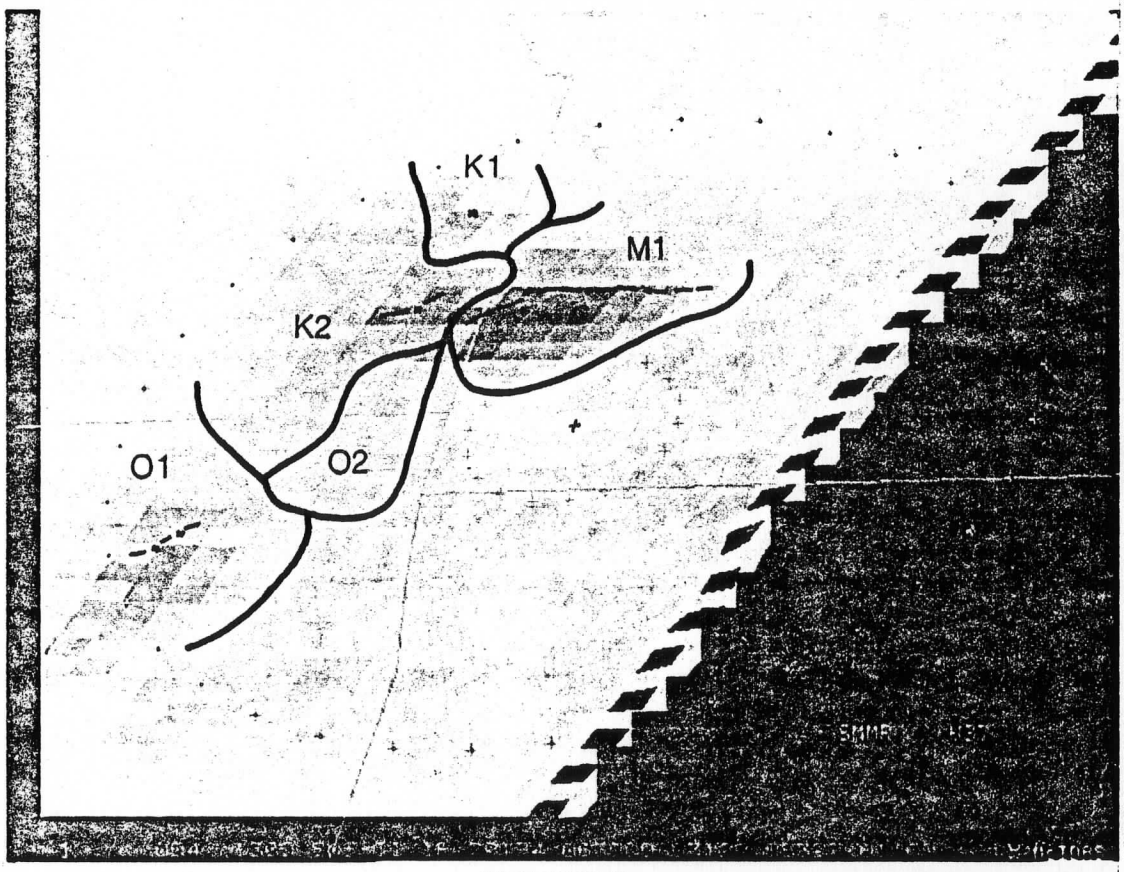

Fig. 15

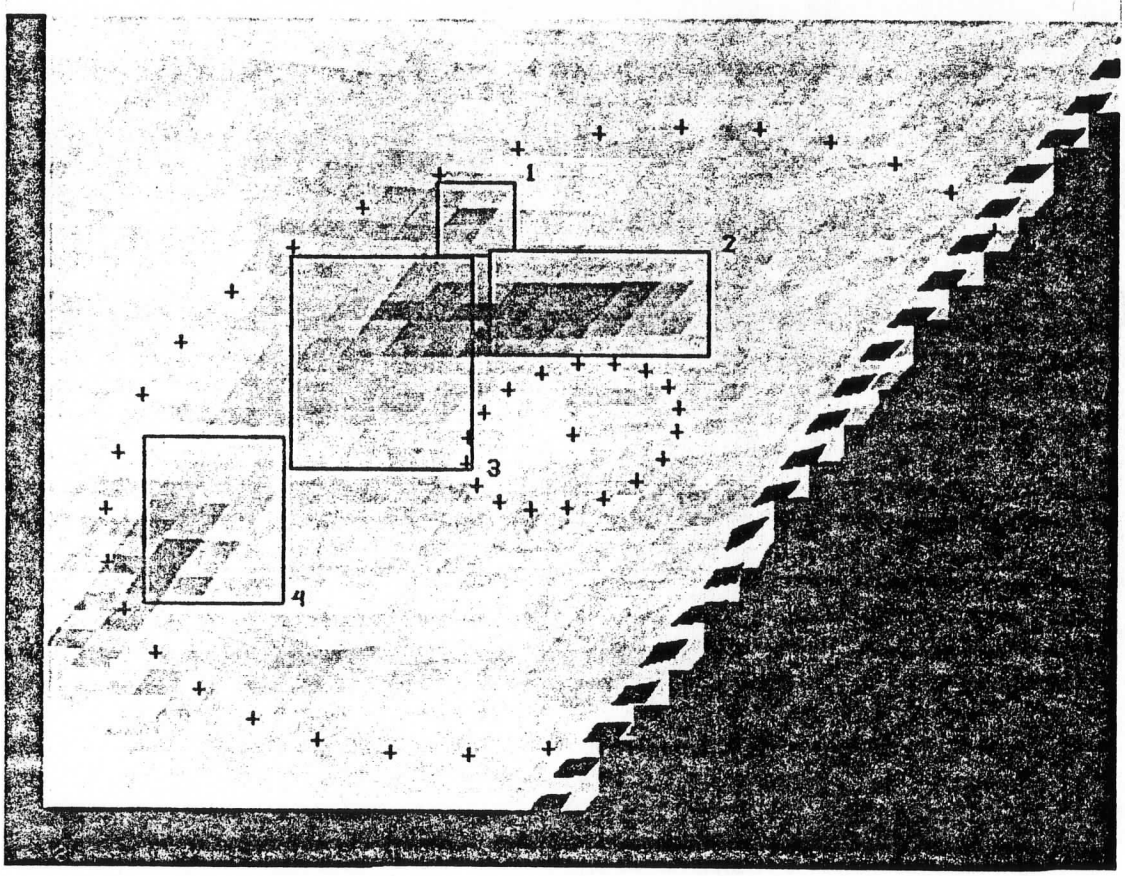

Fig. 16

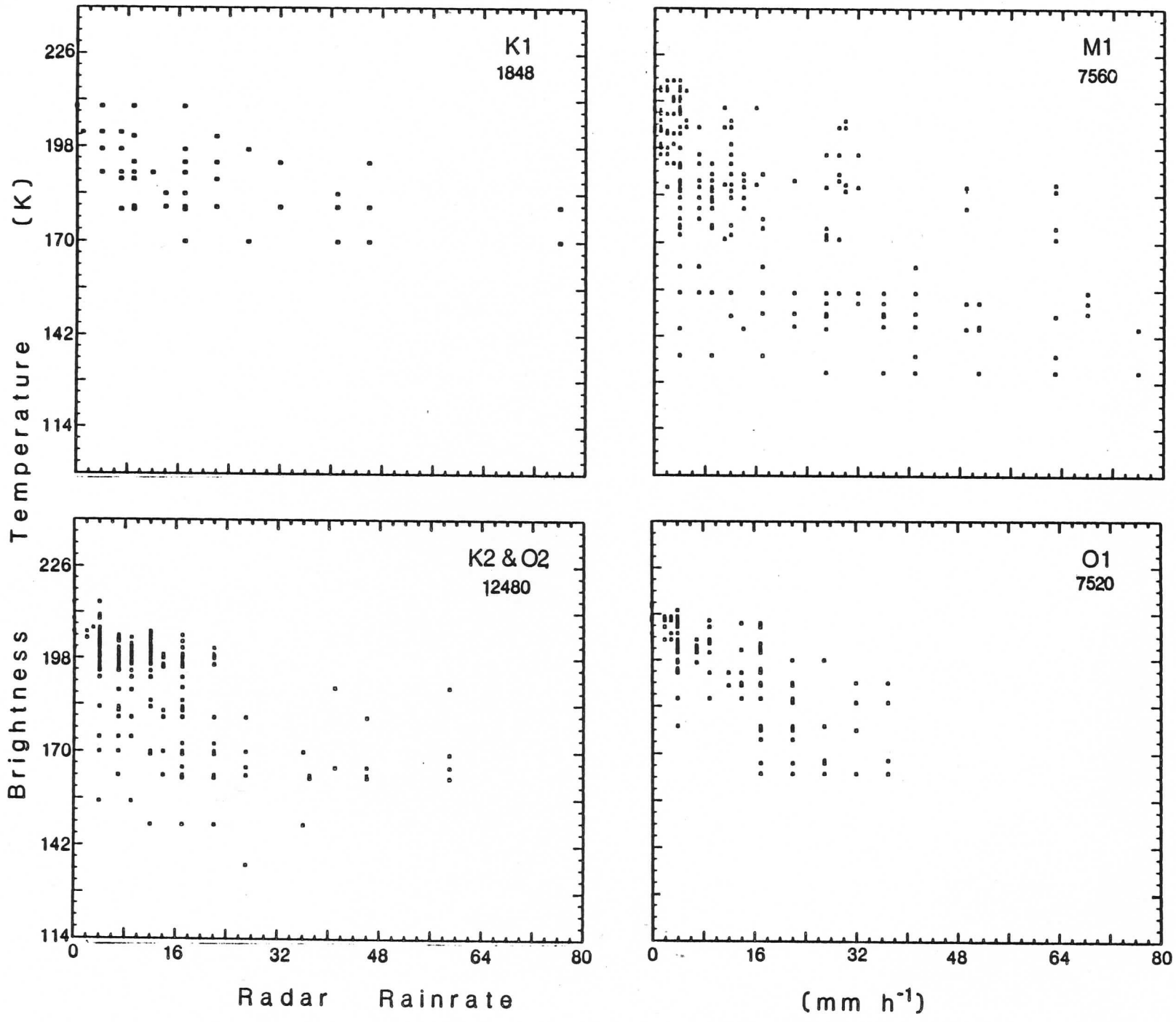
K1
1848
M1
7560
K2 & O2
12480
O1
7520
Brightness Temperature (K)
226
198
170
142
114
0
16
32
48
64
80
Radar Rainrate
(mm h-1)

Fig. 17

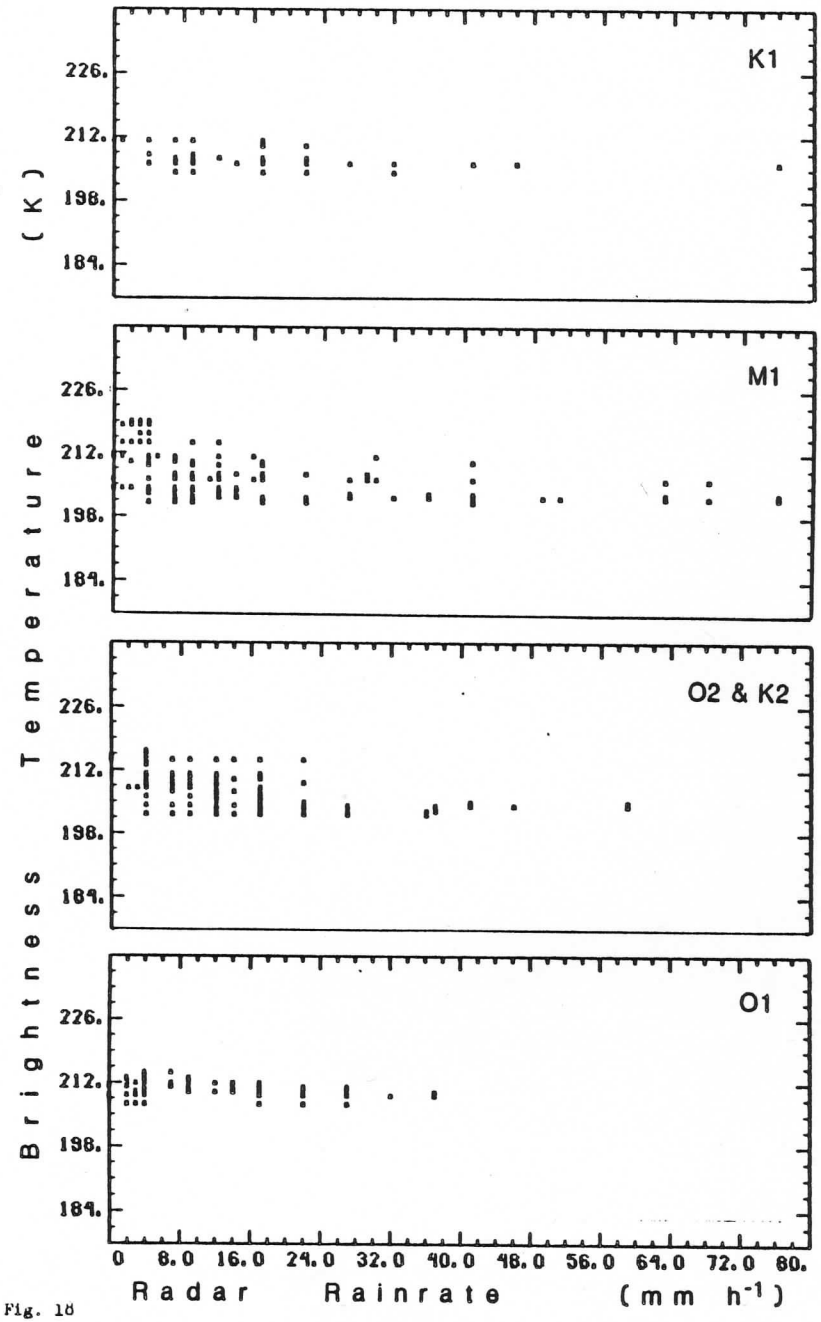
K1
M1
O2 & K2
O1
226.
212.
198.
184.
Brightness Temperature (K)
0 8.0 16.0 24.0 32.0 40.0 48.0 56.0 64.0 72.0 80.
Radar Rainrate (mm h-1)

Fig. 18

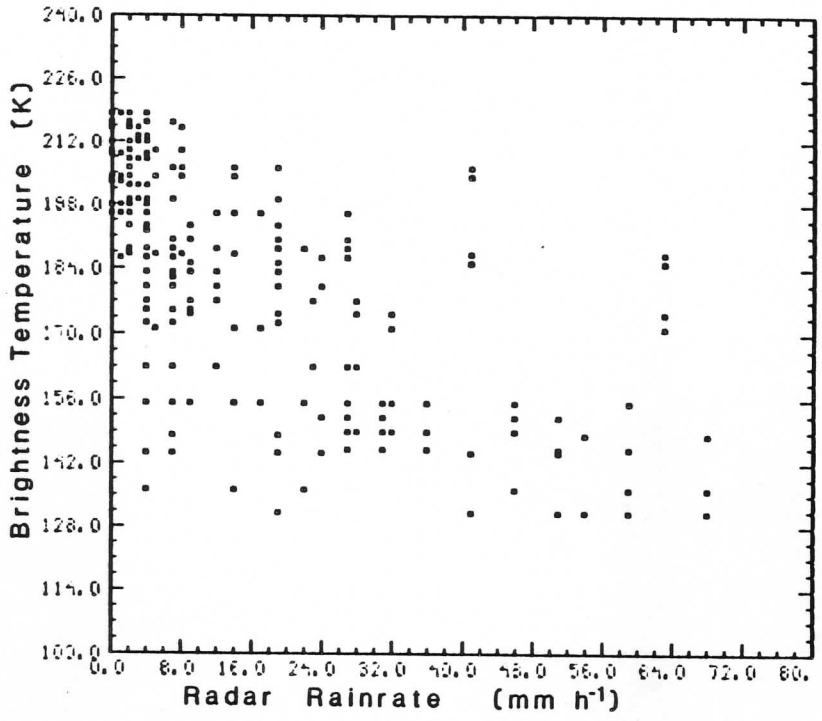
240.0
226.0
212.0
198.0
184.0
170.0
156.0
142.0
128.0
114.0
100.0
Brightness Temperature (K)
0.0 8.0 16.0 24.0 32.0 40.0 48.0 56.0 64.0 72.0 80.
Radar Rainrate (mm h-1)

Fig. 19